A scattering approach to the quantization of Hamiltonians in two dimensions-application to the wedge billiard

1995 J. Phys. A: Math. Gen. 28 77

(http://iopscience.iop.org/0305-4470/28/1/014)

J. Phys. A: Math. Gen. 28 (1995) 77–104. Printed in the UK

A scattering approach to the quantization of Hamiltonians in two dimensions—application to the wedge billiard

C Rouvinez† and U Smilansky‡

† Institut de Physique Théorique, Ecole Polytechnique Fédérale de Lausanne, PHB-Ecublens, CH-1015 Lausanne, Switzerland

‡ Department of Physics of Complex Systems, The Weizmann Institute of Science, Rehovot, 76100 Israel

Received 15 August 1994, in final form 30 September 1994

Abstract. We extend the scattering approach to quantize general Hamiltonian systems in two dimensions and demonstrate it for the wedge billiard. The resulting energy levels are given by the zeros of a secular equation. The corresponding wavefunctions may also be constructed. We verify analytically that this quantization condition is exact in the case of the integrable wedges. This method has been applied successfully to computing numerically a few thousand levels for various values of the angle. Using these data, we can check the Gutzwiller trace formula and other semiclassical relations involving the scattering matrix and periodic orbits, for which we find excellent agreement.

1. Introduction

Since its introduction some years ago, the scattering approach for quantization [1] has been used exclusively to quantize billiards, and for these systems it has proved to be a very convenient starting point for both analytical [2–4] and numerical [5, 6] investigations. Recently, Eckmann and Pillet [7] have proved a theorem which puts one of the versions of the scattering approach on a rigorous foundation. The main purpose of the present work is to show that the scattering approach can be extended quite easily to other systems with Hamiltonians of the form

$$H(r,p)=\frac{p^2}{2m}+V(r) \tag{1}$$

where r (p) are Euclidean coordinates (momenta) in the plane, and it is assumed that $V(r)\to\infty$ for $|r|\to\infty$. We shall show how one can construct two auxiliary scattering systems, in terms of which quantization is achieved. The main result is that here also, one can define a scattering matrix $S(E)$, and determine the spectrum of the original problem by finding the energies E_n at which the spectrum of S contains the eigenvalue 1. Once this is done, one can develop the semiclassical quantization using the same ideas and formalism as were used previously, and derive the semiclassical expression for the spectral density [8], the Gutzwiller Voros ζ function etc.

We shall illustrate this formalism by quantizing a system which can be considered as intermediate between billiards and potential problems of type (1). This is the wedge billiard, which consists of two hard walls that meet at the origin $y=-\cot(\beta_L)x$ and $y=\cot(\beta_R)x$ (the angles are measured away from the y-axis). The motion is bounded by a potential

0305-4470/95/010077+28$19.50

$V(r) = y$. The wedge billiard has a few important advantages: it is known that the classical dynamics are integrable, mixed or hyperbolic depending on the choice of the angles $\beta_{L,R}$. In the chaotic regime with $\beta_L = 0$, the dynamics can be represented symbolically in terms of a binary code. This is of great help in identifying periodic orbits. The quantization of the wedge billiard was previously discussed by Wittek and others [9, 10] and later by Szeredi *et al* [11–14]. This will enable us to compare the more familiar approach, which was previously followed, with the scattering approach which we pursued here. Last but not least, the Hamiltonian is sufficiently simple so that a large quantum database can be calculated. It allows a detailed investigation of the semiclassical approximation and the validity of various assumptions which are made when this approximation is derived.

The paper is arranged in the following way. The first section describes the exact quantization procedure for a general Hamiltonian of the form (1). Once this is done, we shall focus on the wedge billiard, and show how the $S(E)$-matrix is written explicitly in terms of integrals involving Airy functions. A good check is provided for the cases where $\beta_L + \beta_R = \pi/2$ and $\beta_L = 0$, $\beta_R = \pi/4$. These wedge billiards are integrable, and we shall show explicitly that the scattering approach provides the exact energy levels. An important advantage of the scattering approach is that it offers a very efficient procedure for numerical quantization. This will be discussed in section 3, and the accuracy of the method will be studied in detail. The outcome of the numerical work consists of spectra of several thousands of levels each, which form an extensive database for further studies of the semiclassical approximation, which will be the subject of section 4. This section will start with a short résumé of the derivation of the semiclassical approximation for the spectral density (Gutzwiller's trace formula). In section 5, we test numerically the validity of the semiclassical approximations derived in the previous section. Finally, we discuss the possible extensions of this work in the last section.

2. Exact quantization

We consider a two-dimensional system with Hamiltonian of type (1), where motion is bounded by the potential. Here we are looking for the square-integrable solutions $\Psi(x, y)$ of the stationary Schrödinger equation ($\hbar = 1$)

$$\left[-\frac{1}{2m}\Delta + V(x, y) - E\right]\Psi(x, y) = 0 \tag{2}$$

on $\mathbb{R}^2$. To solve this problem, we adapt a method based on scattering theory [1].

First, we take a straight line Γ in the xy-plane. The method applies for an arbitrary Γ, but a sensible choice of the section will reduce the error of the semiclassical approximation. Performing an appropriate rotation of the coordinate system, we can always assume that Γ lies on the y-axis. Thus, it separates the original system into two independent left (L) and right (R) scattering systems. The R system is formed by the potential on the right side of Γ, and its constant continuation on the left side (see figure 1):

$$V_R(x, y) = \begin{cases} V(x, y) & \text{for} \quad x \geqslant 0 \\ V(0, y) & \text{for} \quad x \leqslant 0. \end{cases} \tag{3}$$

Hence motion in the y-direction is bounded by the potential, whereas motion in the x-direction is free for $x \leqslant 0$. The constant potential along the negative x-axis forms a 'waveguide' in which the scattering process is defined. Similarly, we define the L system using the left part of the original system. The corresponding waveguide runs along the positive x-axis. The solutions of the R (L) scattering system are solutions of the stationary

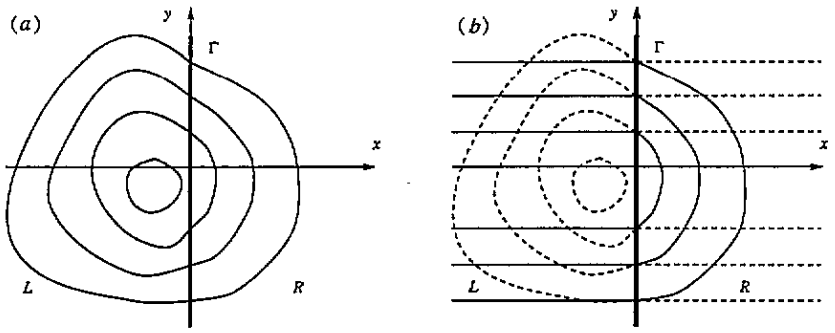

Figure 1. (*a*) Equipotential lines of the original Hamiltonian system. The section Γ is taken on the vertical axis. (*b*) Equipotential lines of the right (full curves) and left (broken curves) scattering systems.

Schrödinger equation restricted to the left (right) side of the origin and the right (left) waveguide. In the asymptotic region $x \leqslant 0$ ($x \geqslant 0$), such solutions may be written

$$\psi_m^{\mathrm{R(L)}}(x, y) = \sum_{l=1}^{\infty} \frac{1}{\sqrt{k_l}} \left[\delta_{ml} \mathrm{e}^{\pm \mathrm{i}k_l x} + S_{ml}^{\mathrm{R(L)}} \mathrm{e}^{\mp \mathrm{i}k_l x}\right] \phi_l(y) \qquad \forall m \in \mathbb{N}^* \tag{4}$$

where the functions $\phi_l(y)$ are channel or mode eigenfunctions with eigen-energies E_l, and

$$k_l = \begin{cases} \sqrt{E - E_l} & \text{for} \quad E \geqslant E_l \\ \mathrm{i}\sqrt{E_l - E} & \text{for} \quad E \leqslant E_l \end{cases} \qquad \text{so that} \quad k_l^2 + E_l = E\,. \tag{5}$$

The channel eigenfunctions $\phi_l(y)$ are the solutions of the one-dimensional Schrödinger equation on Γ:

$$\left[-\frac{1}{2m}\frac{\partial^2}{\partial y^2} + V(0, y) - E_l\right] \phi_l(y) = 0\,. \tag{6}$$

As the potential is binding, the energy spectrum is discrete. The ϕ_l's provide an orthonormal basis of the Hilbert space of the one-dimensional problem. The waveguides are the same for the R and L problems. Note that when the exact solutions of (6) are not known analytically, one can still solve it in the WKB approximation, in order to get a quantization condition which holds in the semiclassical regime.

A channel l for which $k_l \in \mathbb{R}^+$ is called *open* and the corresponding modes *travelling*, since $\mathrm{e}^{\pm \mathrm{i}k_l x}$ represents propagating wavefunctions. When $k_l \in \mathrm{i}\mathbb{R}^+$, $\mathrm{e}^{\pm \mathrm{i}k_l x}$ is an increasing or decreasing exponential function. In that case, one says that the channel l is *closed* and the mode *evanescent*. For potentials bounded from below, the number $\Lambda(E)$ of open channels at fixed energy E is finite, whereas the number of closed channels is infinite. The functions $\mathrm{e}^{\mathrm{i}k_l x}\phi_l(y)$ stand for wavefunctions travelling from $x = -\infty$ into the scattering system. We will call them *incoming modes*. Similarly, the functions $\mathrm{e}^{-\mathrm{i}k_l x}\phi_l(y)$ will be referred as *outgoing modes*. Thus, for $m \leqslant \Lambda$, the function ψ_m^{R} represents a wave of energy E propagating from the left in the incoming open channel m, scattering against the right part of the potential and re-emitted with amplitude S_{ml}^{R} in the various open and closed channels l. The wavefunctions with $m > \Lambda$ do not correspond to propagating modes. They are usually neglected in the semiclassical approximation, since their contributions decrease exponentially in the asymptotic domain. Here we have to consider them, since the wavefunction is expanded on a complete basis on Γ.

We shall use the scattering functions ψ_m^{R} and ψ_m^{L} to construct an eigenfunction of the original Hamiltonian. As Ψ has to satisfy the Schrödinger equation on the R and L sides of Γ, a good ansatz is a function defined by a linear combination of the ψ_m^{R} in the region $x \geqslant 0$, and a linear combination of the ψ_m^{L} in the region $x \leqslant 0$. Such a function does not exist for arbitrary values of the energy, since the wavefunctions of both decompositions and their normal derivatives (with respect to Γ) have to match at $x = 0$. Actually, this matching is the quantization condition. For this purpose we have to find two sets of coefficients a_m^{R} and a_m^{L}, $m \in \mathbb{N}^*$, such that

$$\Psi(x,y) = \begin{cases} \displaystyle\sum_{m=1}^{\infty} a_m^{\mathrm{R}} \psi_m^{\mathrm{R}}(x,y) & \text{for} \quad x \geqslant 0 \\ \displaystyle\sum_{m=1}^{\infty} a_m^{\mathrm{L}} \psi_m^{\mathrm{L}}(x,y) & \text{for} \quad x \leqslant 0 \end{cases} \tag{7}$$

and the values of both the R and the L decompositions of Ψ and $\partial_x \Psi$ have to be matched at $x = 0$. Using the orthonormality of the functions $\phi_l(y)$, this condition transforms into a system of linear equations

$$\begin{aligned} &\sum_{m=1}^{\infty} a_m^{\mathrm{R}} \frac{1}{\sqrt{k_l}} \left[\delta_{ml} + S_{ml}^{\mathrm{R}}\right] = \sum_{m=1}^{\infty} a_m^{\mathrm{L}} \frac{1}{\sqrt{k_l}} \left[\delta_{ml} + S_{ml}^{\mathrm{L}}\right] \qquad \forall l \in \mathbb{N}^* \\ &\mathrm{i} \sum_{m=1}^{\infty} a_m^{\mathrm{R}} \sqrt{k_l} \left[\delta_{ml} - S_{ml}^{\mathrm{R}}\right] = \mathrm{i} \sum_{m=1}^{\infty} a_m^{\mathrm{L}} \sqrt{k_l} \left[-\delta_{ml} + S_{ml}^{\mathrm{L}}\right] \qquad \forall l \in \mathbb{N}^* \end{aligned} \tag{8}$$

which is a set of homogeneous equations for the coefficients a^{R} and a^{L}. Using a matrix notation and remembering that scattering matrices are symmetric (see appendix A), we obtain the matching condition in the form

$$\begin{pmatrix} \mathbb{1} & -S^{\mathrm{L}} \\ -S^{\mathrm{R}} & \mathbb{1} \end{pmatrix} \begin{pmatrix} a^{\mathrm{R}} \\ a^{\mathrm{L}} \end{pmatrix} = 0 \tag{9}$$

which admits a non-trivial solution if and only if

$$\mathrm{Ker}\left[\mathbb{1} - S(E)\right] \neq \emptyset \qquad \text{with} \qquad S(E) = S^{\mathrm{L}} \cdot S^{\mathrm{R}}. \tag{10}$$

Thus the system admits E as eigen-energy whenever $S(E)$ has an eigenvalue $+1$. Since each element of the kernel gives a different solution for the matching, the degeneracy simply corresponds to this number of elements. Furthermore, this quantization condition gives a constructive method to obtain not only the eigen-energies, but the wavefunction too. First, one has to look for a value of E such that (10) is satisfied. Then one solves (9) to obtain the coefficients of the decomposition (7).

For symmetrical systems, it is also possible to determine the parity of the wavefunction. Consider a system for which the section Γ is a symmetry line with

$$V(x,y) = V(-x,y) \qquad \forall x \in \mathbb{R}. \tag{11}$$

As both the R and the L scattering systems are identical, $S^{\mathrm{R}} = S^{\mathrm{L}}$. According to (10), the system admits an eigenfunction of energy E each time $S^{\mathrm{L}} \cdot S^{\mathrm{R}}$ has an eigenvalue $+1$. Thus the symmetric system will have eigenfunctions for each eigenvalue ± 1 of S^{R}. For this special case, the system (8) can be simplified and rewritten as

$$\left[\mathbb{1} + S^{\mathrm{R}}\right]\left(a^{\mathrm{R}} - a^{\mathrm{L}}\right) = 0 \qquad \left[\mathbb{1} - S^{\mathrm{R}}\right]\left(a^{\mathrm{R}} + a^{\mathrm{L}}\right) = 0. \tag{12}$$

Assume $S^{\mathrm{R}}(E)$ has an eigenvalue $+1$. The corresponding eigenvector $(a^{\mathrm{R}} + a^{\mathrm{L}})$ must also satisfy the other equation of the system, so that $a^{\mathrm{R}} = a^{\mathrm{L}}$. From (7), one deduces that

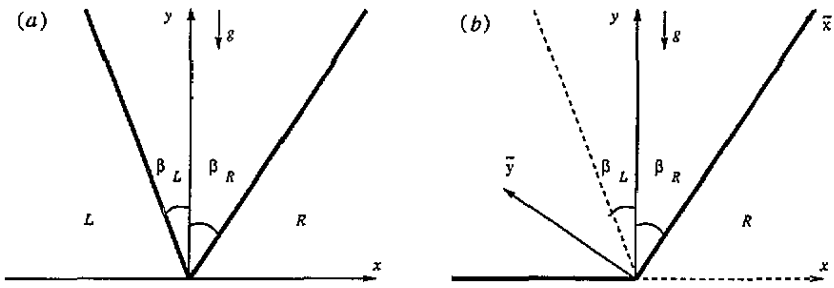

Figure 2. (*a*) Original billiard system composed of two inclined sides. (*b*) Right scattering system (full lines) composed of the right inclined side and a waveguide on the negative x-axis. Left scattering system (broken lines) composed of the left inclined side and a waveguide on the positive x-axis.

$\Psi(x, y) = \Psi(-x, y)$, i.e. that the corresponding wavefunction is symmetric. Similarly, the eigenvalues -1 of $S^{\mathrm{R}}(E)$ lead to antisymmetric eigenfunctions verifying $\Psi(x, y) = -\Psi(-x, y)$.

At this point we depart from the general Hamiltonian (1) and consider the wedge billiard. This billiard consists of two walls (infinite potential barrier) along the lines $y = -\cot(\beta_{\mathrm{L}})x$ and $y = \cot(\beta_{\mathrm{R}})x$ (see figure 2(*a*)). The motion is bounded by a gravitational potential and the Hamiltonian of the system reads (using units where $m = g = 1$)

$$H = \frac{p_x^2}{2} + \frac{p_y^2}{2} + y\,. \tag{13}$$

The only parameters determining the behaviour of the system are the angles β_{L} and β_{R} between the sides of the wedge. This system is integrable when $\beta_{\mathrm{L}} + \beta_{\mathrm{R}} = \pi/2$ and $\beta_{\mathrm{L}} = 0$, $\beta_{\mathrm{R}} = \pi/4$. Wojtkowski [15] has shown analytically that this system admits an almost everywhere non-vanishing Lyapunov exponent for $\beta_{\mathrm{L}} + \beta_{\mathrm{R}} > \pi/2$. Hence, for these values of the parameters, it is ergodic and all isolated periodic orbits are unstable.

Here we are looking for the solutions of the stationary Schrödinger equation with Dirichlet boundary condition on the wedge. We take the section Γ directly on the y-axis. The R system is formed by the right side of the wedge and the reflecting wall along the negative x-axis (see figure 2(*b*)). The motion in the y-direction is bounded by the potential and the reflecting wall, whereas motion in the x-direction is free. The combination of the reflecting wall and the linear potential forms the waveguide along the negative x-axis. The L system is defined in the same way, using the left side of the wedge and a waveguide on the positive x-axis. The channel eigenfunctions are discussed in appendix B.

To find the scattering matrix S^{R} of the right scattering system we will expand the wavefunctions ψ_m^{R} on another basis on the right side of the vertical axis, and once again use the matching condition at $x = 0$. In the domain $x \geqslant 0$, the right scattering system is separable when expressed in rotated coordinates $\tilde{x}\tilde{y}$ directed along the inclined boundary. Thus a natural basis is given by a product of two Airy functions (see appendix B) vanishing at $\tilde{y} = 0$:

$$\begin{aligned}\varphi_r &= \mathrm{Ai}\left[(2s)^{1/3}\tilde{y} + z_r\right] \mathrm{Ai}\left[(2c)^{1/3}\tilde{x} - \left(2^{1/3}E + s^{2/3}z_r\right)c^{-2/3}\right] \\ &= \mathrm{Ai}\left[(2s)^{1/3}(-cx + sy) + z_r\right] \mathrm{Ai}\left[(2c)^{1/3}(sx + cy) - \left(2^{1/3}E + s^{2/3}z_r\right)c^{-2/3}\right]\end{aligned} \tag{14}$$

where z_r ($r \in \mathbb{N}^*$) is the rth zero of the Airy function Ai, $c = \cos(\beta_R)$ and $s = \sin(\beta_R)$. Each ψ_m^R can be expressed as a linear combination of the φ_r's

$$\psi_m^R(x, y) = \sum_{r=1}^{\infty} J_{mr} \varphi_r(x, y) \tag{15}$$

and the matching condition between both decompositions of ψ_m^R at $x = 0$ reads

$$\begin{aligned} \sum_{l=1}^{\infty} \frac{1}{\sqrt{k_l}} \left[\delta_{ml} + S_{ml}^R\right] \phi_l(y) &= \sum_{r=1}^{\infty} J_{mr} \varphi_r(0, y) \\ \sum_{l=1}^{\infty} i\sqrt{k_l} \left[\delta_{ml} - S_{ml}^R\right] \phi_l(y) &= \sum_{r=1}^{\infty} J_{mr} \left(\partial_x \varphi_r\right)(0, y) \end{aligned} \tag{16}$$

where the coefficients S_{ml}^R and J_{mr} are the unknowns. Multiplying by $\phi_n(y)$, integrating over y and using the orthonormality of the ϕ_n's, this transforms into

$$\begin{aligned} \delta_{mn} + S_{mn}^R &= \sum_{r=1}^{\infty} J_{mr} I_{rn}^1 \\ \delta_{mn} - S_{mn}^R &= \sum_{r=1}^{\infty} J_{mr} I_{rn}^2 \end{aligned} \tag{17}$$

where

$$\begin{aligned} I_{rn}^1 &= \sqrt{k_n} \int_0^{\infty} \varphi_r(0, y)\, \phi_n(y)\, dy \\ I_{rn}^2 &= \frac{-i}{\sqrt{k_n}} \int_0^{\infty} \left(\partial_x \varphi_r\right)(0, y)\, \phi_n(y)\, dy\,. \end{aligned} \tag{18}$$

Finally, system (17) can be simplified and rewritten in the following matrix form:

$$\begin{aligned} S^R &= J \cdot I^- \\ \mathbb{1} &= J \cdot I^+ \end{aligned} \qquad \text{with} \quad I^{\pm} = \tfrac{1}{2}\left(I^1 \pm I^2\right). \tag{19}$$

Equation (19) does not ensure that J is the inverse of I^+, since both matrices are infinite-dimensional. The scattering matrix S^L of the left scattering system is determined in the same way.

For systems with $\beta_L = \beta_R$, we have $S^L = S^R$ and the secular equation can be simplified. Using (17), we have

$$\begin{aligned} \mathrm{Det}\left[\mathbb{1} + S^R\right] &= \mathrm{Det}\left[J\right]\mathrm{Det}\left[I^1\right] \\ \mathrm{Det}\left[\mathbb{1} - S^R\right] &= \mathrm{Det}\left[J\right]\mathrm{Det}\left[I^2\right] \end{aligned} \tag{20}$$

and the problem reduces to finding the zeros of $\mathrm{Det}\left[J\right]$, $\mathrm{Det}\left[I^1\right]$ and $\mathrm{Det}\left[I^2\right]$. Replacing (15) in (7) and permuting the sums, we obtain

$$\Psi(x, y) = \sum_{r=1}^{\infty} \left(\sum_{m=1}^{\infty} a_m^R J_{mr} \right) \varphi_r(x, y) \tag{21}$$

so that an eigenvector of J^T with eigenvalue 0 (if it exists) would lead to an identically vanishing wavefunction. Hence it is enough to locate the solutions of the equations

$$\mathrm{Det}\left[I^1(E)\right] = 0 \qquad \text{and} \qquad \mathrm{Det}\left[I^2(E)\right] = 0\,. \tag{22}$$

Once an eigen-energy E_n has been found, the corresponding wavefunction reads

$$\Psi(x, y) = \sum_{r=1}^{\infty} b_r \varphi_r(x, y) \tag{23}$$

where b is the element of the kernel of $[I^1(E_n)]^{\mathrm{T}}$ for antisymmetric eigenmodes or the element of the kernel of $[I^2(E_n)]^{\mathrm{T}}$ for symmetric eigenmodes.

As a first illustration of this method, we apply it to the integrable case with $\beta_{\mathrm{L}} = \beta_{\mathrm{R}} = \pi/4$. The system is separable in the rotated coordinates $\tilde{x}\tilde{y}$. The eigenfunctions are products of the eigenfunctions of the one-dimensional bouncer (see appendix B with $g_{\tilde{x}} = g_{\tilde{y}} = 2^{-1/2}$)

$$\Psi_{ml}(\tilde{x}, \tilde{y}) = K_{ml} \operatorname{Ai}\left[2^{1/6}\tilde{x} + z_m\right] \operatorname{Ai}\left[2^{1/6}\tilde{y} + z_l\right] \qquad \forall m, l \in \mathbb{N}^* \tag{24}$$

where $K_{ml} = 2^{1/6}\left(\operatorname{Ai}'[z_m]\operatorname{Ai}'[z_l]\right)^{-1}$ is the normalization constant. The related eigen-energies read

$$E_{ml} = -2^{-2/3}(z_m + z_l)\,. \tag{25}$$

As E_{ml} is symmetric in m and l, it is degenerate for $m \neq l$. Evaluation of $I^1_{mn}(E)$ at $E = E_{ml}$ gives

$$\begin{aligned} I^1_{mn}(E_{ml}) &= \sqrt{k_n} \int_0^{\infty} \operatorname{Ai}\left[2^{-1/3}y + z_m\right] \operatorname{Ai}\left[2^{-1/3}y - 2^{2/3}E_{ml} - z_m\right] \phi_n(y)\,\mathrm{d}y \\ &= \sqrt{k_n} \int_0^{\infty} \operatorname{Ai}\left[2^{-1/3}y + z_m\right] \operatorname{Ai}\left[2^{-1/3}y + z_l\right] \phi_n(y)\,\mathrm{d}y \\ &= I^1_{ln}(E_{ml}) \qquad \forall n \in \mathbb{N}^*\,. \end{aligned} \tag{26}$$

Thus the mth and lth rows of $I^1(E_{ml})$ are equal. A similar computation of $I^2_{mn}(E)$ at $E = E_{ml}$ yields

$$I^2_{mn}(E_{ml}) = -I^2_{ln}(E_{ml}) \qquad \forall n \in \mathbb{N}^* \tag{27}$$

which shows that the mth and lth rows of $I^2(E_{ml})$ differ only by a sign. As $I^2_{mn}(E_{mm}) = -I^2_{mn}(E_{mm}) = 0$ for all $n \in \mathbb{N}^*$, $\operatorname{Ker}\left[I^2(E_{mm})\right] \neq \emptyset$. $S^{\mathrm{R}}(E_{mm})$ has an eigenvalue $+1$ at $E = E_{mm}$ and the system admits a non-trivial symmetric solution

$$\left.\begin{array}{ll} b_m & \neq 0 \\ b_i & = 0 \quad \text{for } i \neq m \end{array}\right\} \quad \Rightarrow \quad \Psi(x, y) = \varphi_m(x, y) \tag{28}$$

as expected for this energy. For $m \neq l$, $\operatorname{Ker}\left[I^2(E_{ml})\right] \neq \emptyset$ and $\operatorname{Ker}\left[I^1(E_{ml})\right] \neq \emptyset$. Thus $S^{\mathrm{R}}(E_{ml})$ has one eigenvalue $+1$ and another -1 at $E = E_{ml}$. The system of equations has two different non-trivial solutions

$$\left.\begin{array}{ll} b_m & = \pm b_l \\ b_i & = 0 \quad \text{for } i \notin \{m, l\} \end{array}\right\} \quad \Rightarrow \quad \Psi(x, y) = \varphi_m(x, y) \pm \varphi_l(x, y) \tag{29}$$

and the energy level is degenerate. The solutions correspond respectively to a symmetric and an antisymmetric eigenmode of the billiard.

For the integrable wedge with $\beta_{\mathrm{L}} = 0$ and $\beta_{\mathrm{R}} = \pi/4$, we have $S^{\mathrm{L}} = -\mathbb{1}$. The secular equation transforms into $\operatorname{Det}\left[\mathbb{1} + S^{\mathrm{R}}\right] = 0$. Thus one has to consider only the above antisymmetric solutions vanishing on the vertical boundary.

In order to complete the discussion of the integrable wedge billiards, the general case with $\beta_{\mathrm{L}} + \beta_{\mathrm{R}} = \pi/2$ is investigated in appendix C, where the section $\tilde{\Gamma}$ is taken on the inclined side of the wedge.

3. Numerical results

In this section we show how to implement the scattering method to determine the energy levels and the wavefunctions when $\beta_L = 0$ and $\beta_R \neq \pi/4$. We also discuss the accuracy of these results and the efficiency of the method.

The S-matrix is an infinite-dimensional matrix. Only in the case $\beta_R = \pi/4$ is it possible to treat the full S-matrix analytically. For other values of β_R, we have to consider restrictions of S with finite numbers of elements. The main problem in practical computations is to find the optimal restriction which will yield the required accuracy at the minimum computational effort. We show in appendix A that S is unitary with respect to the subspace of open channels. They contain the most important part of the information, since they represent travelling modes which give the leading contribution to the semiclassical limit. Thus, we have to consider at least the restriction to the subspace of the open channels. Unfortunately, such a truncation of S will miss some eigenvalues. This is well illustrated by the integrable case $\beta_L = 0$ and $\beta_R = \pi/4$ at $E = E_{mn}$ with $n = 1$. To see that the first and the mth row of I^1 are equal, the dimension of the restriction of S must be at least m. But due to the inclination of the boundary, we may have $m \simeq \Lambda/\sin(\beta_R)$. Hence it is necessary to include $\Lambda(\mathrm{cosec}(\beta_R) - 1)$ evanescent modes to reproduce all levels of the integrable case. Such a phenomenon might happen whenever both the $\psi_m^R(x, y)$ and the $\varphi_r(x, y)$ basis do not have the same number of elements which contribute semiclassically. This clearly demonstrates the need for including some closed channels in the computations to obtain a precise and reliable spectrum. On the other hand, the size of the elements of S which involve closed channels decreases steadily at a rate which is slower than exponential, but seems to be faster than a power law. Hence, including too many evanescent modes leads to numerical imprecision. However, as we have no analytical method to estimate the number of evanescent modes which guarantees a desired accuracy, we have to investigate this problem numerically.

In figure 3 we plot the mean error in the zeros of the secular equation as a function of the number of evanescent modes. The mean is taken over the 100 lowest eigen-energies for $\beta_R = \pi/3$, and the error is given in units of the mean level spacing. The gain in precision is higher when adding the first and second non-propagating modes. This might be a consequence of the difference between both decompositions of Ψ, as explained above. Although the number of points is small, the error seems to decrease exponentially when more than two channels are added. Thus the algorithm converges very rapidly when the number of closed channels is increased. In what follows, we assume that the values to which the zeros tend are the exact eigen-energies.

We have pointed out above that the truncation of the space of evanescent modes might lead to missing some eigen-energies. To check this point we studied the integrated density

$$N(E) = \sum_{n=1}^{\infty} \theta(E - E_n) \tag{30}$$

and its fluctuations around its averaged value [13]

$$N_{AV}(E) = \frac{\tan(\beta_R)}{12\pi} E^3 - \frac{1 + \sec(\beta_R)}{3\sqrt{2}\pi} E^{3/2} + \frac{1}{6} \tag{31}$$

in which the constant term has been postulated to be the same as for billiards with smooth boundary in spite of the corner. The full curve in figure 4 represents a plot of the difference $N_{AV}(E) - N(E)$ for 200 levels starting at the 2000th eigen-energy when $\beta_R = \pi/3$. One expects this quantity to fluctuate around the number of missing levels. The broken curve is

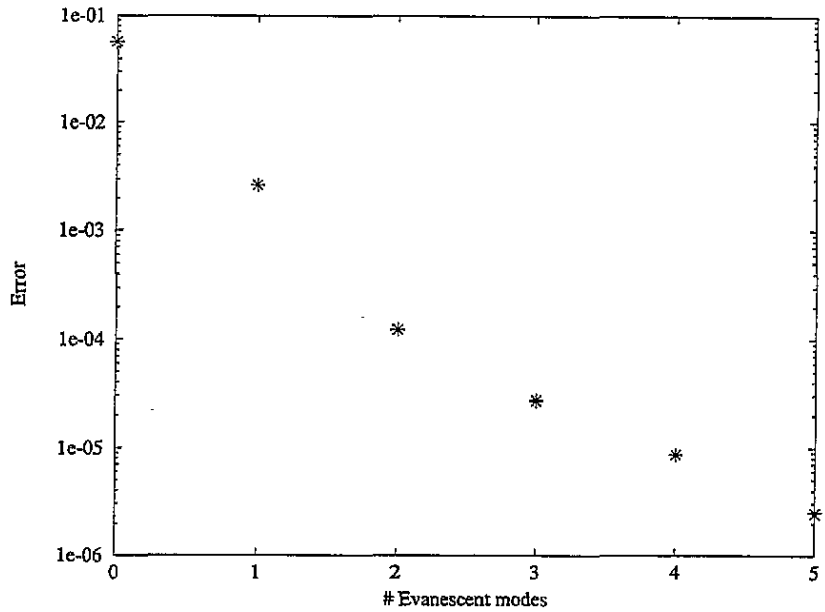

Figure 3. Error in the position of the levels as a function of the number of evanescent modes for $\beta_L = 0$ and $\beta_R = \pi/3$. The error decreases exponentially with the number of evanescent modes.

the corresponding running average over 200 values. Its small value shows that no level is missed, and seems to confirm the choice of the constant term $\frac{1}{6}$ in N_{AV}. The chain curve, which is the running standard deviation from the running average, reflects the strong rigidity of the spectrum, as expected for a chaotic system. The number of open modes $\Lambda(E)$ for large E may be approximated from (B4) and the asymptotic behaviour of z_n for large n [16]. As the leading term of N_{AV} goes like E^3, we obtain

$$\Lambda \sim E^{3/2} \sim \sqrt{N_{AV}}\,. \tag{32}$$

Thus the dimension of the restricted S only increases as the square root of the number of levels, which renders this algorithm efficient. For instance, $\Lambda = 45$ for the 1000th levels of a wedge with $\beta_R = \pi/3$. This allows the computation of relatively high energy levels.

We did not encounter any numerical difficulty in the determination of the first 3300 eigen-energies of the wedge with $\beta_R = \pi/3$. The computation time is highly dependent on the ability to locate the next zero of $\mathrm{Det}\left[I^1(E)\right]$. For energies of this order, computation of I^1 becomes time consuming, since one has to evaluate Λ^2 integrals numerically. This is the only impediment which prevented us from extending the calculations for higher energies. However, the additional $\Lambda(\mathrm{cosec}(\beta_R) - 1)$ evanescent modes might be another source of numerical problems for much higher energies. The elements of I^1_{rn} tend to 0 for $n, r \to \infty$. Thus, if one considers too many evanescent modes, the determinant becomes numerically identical to zero.

Next we discuss the restriction S_{sq} with no evanescent modes, which is the starting point of all the semiclassical theory based on scattering. It is called the *semiquantal* approximation, because it neglects the modes which do not have a classical analogue. The matrix S_{sq} is a $\Lambda \times \Lambda$ matrix for which the quantization condition (10) may be written as

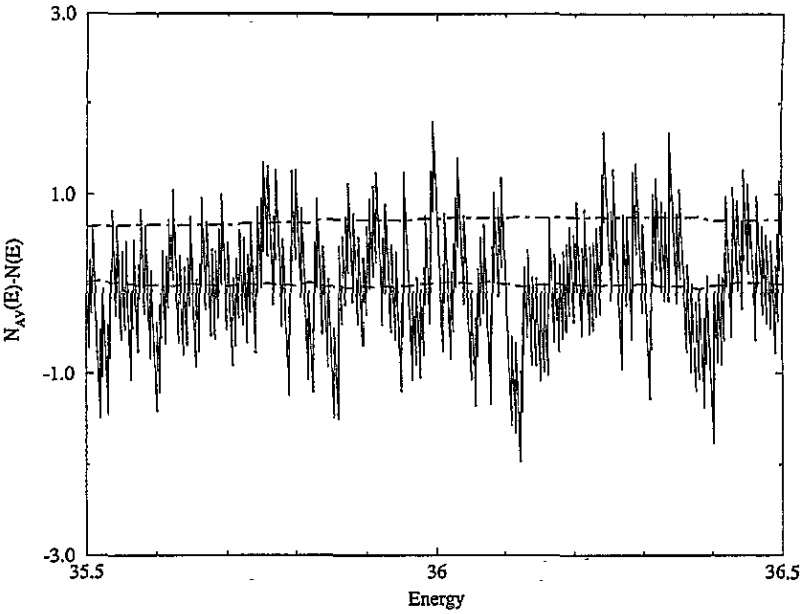

Figure 4. Fluctuations of the exact density $N(E)$ around its averaged value $N_{AV}(E)$ for $\beta_L = 0$ and $\beta_R = \pi/3$. The broken curve indicates the running average over 200 values, and the chain curve the running standard deviation.

the secular equation

$$Z_{sq}(E) = \mathrm{Det}\left[\mathbb{1} - S_{sq}(E)\right] = 0. \tag{33}$$

Figure 5 represents the shift in the position of all the zeros of the semiquantal approximation with 13 and 14 open channels for $\beta_R = \pi/3$. The error is measured with respect to the exact position of the levels in units of the mean levels spacing. The thresholds of the 13–15 channels are marked by broken lines. Comparison with results obtained for other billiards with the same method [1, 6] reveals that the error is some order of magnitude larger for the wedge billiard. This is mainly due to the corner made by the waveguide and the boundary at $x = 0$, because the evanescent modes are essential for the proper description of the wavefunction near such a singularity. This problem does not appear for the above-mentioned billiards where the waveguides were chosen to match the boundary smoothly. However, one can see on this figure that the shift reaches its maximum just before the opening of a new channel, emphasizing the role played by the almost conducting mode. As mentioned above, a more serious drawback of the semiquantal approximation is that it might miss or add some eigenvalues. For instance, the secular equation for $\beta_R = \pi/3$ and $E \leqslant E_{300}$ cannot locate 10 (3.3%) of the eigen-energies and generates 6 (2%) irrelevant ones.

Computation of the S-matrix from (19) involves the inversion of a finite approximation of the matrix I^+, which is a further source of numerical imprecision. The accuracy of the numerical S-matrix can be verified with the help of the relations derived in appendix A. A reasonable estimate of the error is the mean over the difference $S_{oo} \cdot S_{oo}^{\dagger} - \mathbb{1}$, where S_{oo} represents the unitary part of S. We chose to verify the accuracy of S_{oo}, since this part is the relevant one for the semiclassical analysis. In figure 6 we plot the error in the unitary part of $S(E)$ as a function of the number of evanescent modes for $E = E_{10}$ at $\beta_R = \pi/3$. As

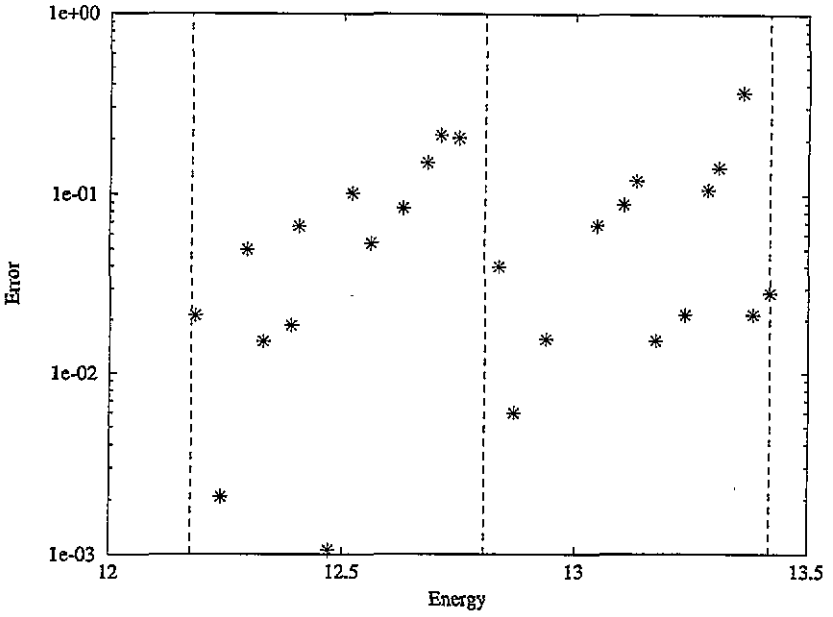

Figure 5. Shift in the position of the zeros corresponding to the semiquantal approximation for $\beta_L = 0$ and $\beta_R = \pi/3$. The maximum is obtained just before the opening of a new channel.

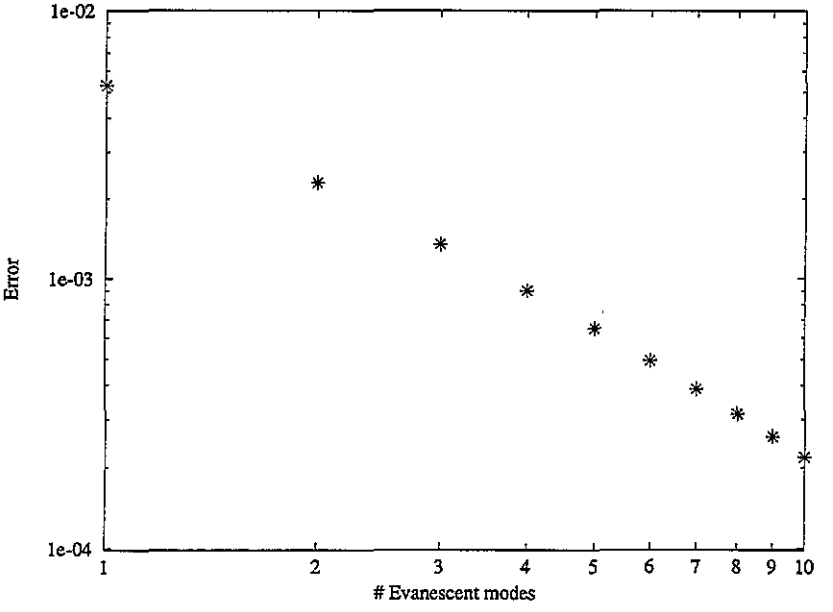

Figure 6. Estimation of the error in the computation of the unitary part of the S-matrix as a function of the number of evanescent modes for $\beta_L = 0$ and $\beta_R = \pi/3$. The error decreases in a power law with the number of evanescent modes.

one can see, the error only decreases as a power law in this case. Notice that $S_{oo} \cdot S_{oo}^* = \mathbb{1}$ is a symmetry which follows automatically from (19) and hence is always satisfied.

4. Semiclassical analysis

Starting from the scattering formalism, we will re-derive the well known semiclassical trace formula for the density of states

$$d(E) = \sum_{n=1}^{\infty} \delta(E - E_n). \tag{34}$$

First we want to take advantage of the unitarity of $S_{sq}(E)$ to rewrite the semiquantal determinant (33) away from the threshold energies as a phase times an amplitude. Using the notation $e^{i\theta_l(E)}$ for the Λ eigenvalues of $S_{sq}(E)$, we may write

$$Z_{sq}(E) = \exp\left[\frac{i\Theta(E)}{2}\right] 2^{\Lambda} \prod_{l=1}^{\Lambda} \sin\left[\frac{\theta_l(E)}{2}\right] \tag{35}$$

where $\Theta(E) = \sum_{l=1}^{\Lambda} \theta_l(E) - \Lambda\pi$. The last product is real on the real energy axis. Therefore, the imaginary part of its logarithmic derivative, calculated at $E + i\epsilon$ in the limit $\epsilon \searrow 0$ is a sum of delta functions located at the eigen-energies. Using the expansion

$$\log \mathrm{Det}\left[\mathbb{1} - S_{sq}(E)\right] = -\sum_{n=1}^{\infty} \frac{1}{n} \mathrm{Tr}\, S_{sq}^n(E) \tag{36}$$

we obtain a semiquantal approximation for the exact density $d(E)$

$$d_{sq}(E) = \frac{1}{2\pi} \frac{\partial}{\partial E} \Theta(E) + \frac{1}{\pi} \lim_{\varepsilon \to 0} \mathrm{Im} \left[\sum_{n=1}^{\infty} \frac{1}{n} \frac{\partial}{\partial E} \mathrm{Tr}\, S_{sq}^n(E + i\varepsilon) \right]. \tag{37}$$

The first term on the RHS corresponds to the smooth part of the density. The Wigner delay time [17] is defined as

$$\tau(E) = \mathrm{Tr}\left[\frac{1}{i\Lambda} S_{sq}^{\dagger}(E) S_{sq}'(E)\right] = \frac{1}{\Lambda} \sum_{l=1}^{\Lambda} \theta_l'(E) \tag{38}$$

where the prime stands for differentiation with respect to E. Thus, this quantity characterizing the scattering is connected to the mean levels density of the billiard via

$$d_{AV}(E) \approx \frac{1}{2\pi} \Theta'(E) = \frac{1}{2\pi} \sum_{l=1}^{\Lambda} \theta_l'(E) = \frac{\Lambda}{2\pi} \tau(E). \tag{39}$$

Integrating over E, we obtain an expression for the mean integrated density

$$N_{AV}(E) \approx \frac{1}{2\pi} \Theta(E) + \text{constant}. \tag{40}$$

Because of the piecewise constant term $-\Lambda\pi$ in the definition of $\Theta(E)$, this expression with constant $= 0$ is valid over the whole range of energy. The second term on the RHS represents the oscillatory part of the density $d_{osc}(E) = d(E) - d_{AV}(E)$. Notice that it only depends on the quantities $\mathrm{Tr}\, S_{sq}^n(E)$ which play a major role in this formalism.

Up to this point we remained at the semiquantal level where all information comes from the quantum description of the system. The next step in the derivation of the semiclassical quantization is to express these quantities in terms of the periodic orbits of the corresponding classical system. Here it is important to note that the scattering matrix is the quantum analogue of the Poincaré map on the matching line Γ [18]. Let us define conjugate action and angle variables (I, ϕ) on Γ. The Poincaré map is the classical transformation which maps the initial condition (I_i, ϕ_i) onto $(I_f, \phi_f) = M(I_i, \phi_i)$ corresponding to the next

intersection of the classical trajectory with the section Γ. The classical dynamics may also be represented by the generating function (or action) $\Phi(E, \phi_i, \phi_f)$ which depends on the energy as a parameter. The mapping is expressed explicitly as

$$I_i = -\frac{\partial \Phi}{\partial \phi_i} \qquad \text{and} \qquad I_f = \frac{\partial \Phi}{\partial \phi_f}. \tag{41}$$

The S-matrix is the analogue of the classical mapping: it maps incoming scattering states onto outgoing scattering states of the system. We shall use this correspondence for wedges where the dynamics is either hyperbolic or integrable.

When the map is hyperbolic, the trace of the semiquantal scattering matrix can be approximated by a sum over isolated periodic orbits [19]

$$\operatorname{Tr} S_{sq}^n(E) \approx \sum_{\{\gamma \,|\, n_\gamma r_\gamma = n\}} \frac{n_\gamma \exp[\mathrm{i} r_\gamma \{\Phi_\gamma(E) - \nu_\gamma \pi/2\}]}{\sqrt{|\operatorname{Det}[\mathbb{1} - (\partial M_\gamma)^{r_\gamma}]|}} \tag{42}$$

where $\Phi_\gamma(E) = \sum_{j=1}^{n_\gamma} \Phi(E, \phi_{j-1}, \phi_j)$ is the action of the periodic orbit γ (setting $\phi_{n_\gamma} = \phi_0$). The quantity ν_γ stands for the Maslov index [20], and ∂M_γ is the monodromy matrix. The sum runs over all isolated primitive periodic orbits γ of the billiard which cross n_γ times the section Γ, and which satisfy $n_\gamma r_\gamma = n$, where r_γ is the number of repetitions. Due to this restriction, generally only a finite number of periodic orbits contribute to this sum for each value of n. Inserting (42) in (37), we obtain a semiclassical approximation for the spectral density in terms of the periodic orbits. Noting that the double sum over all integers n and over the orbits γ such that $n_\gamma r_\gamma = n$ may be replaced by a double sum over all orbits and their repetitions r, we finally get

$$d(E) \approx d_{AV}(E) + \operatorname{Re}\left[\sum_\gamma \sum_{r=1}^{\infty} \frac{T_\gamma(E)}{\pi} \frac{\exp[\mathrm{i} r\{\Phi_\gamma(E) - \nu_\gamma \pi/2\}]}{\sqrt{|\operatorname{Det}[\mathbb{1} - (\partial M_\gamma)^r]|}}\right] \tag{43}$$

where $T_\gamma(E) = \frac{\partial}{\partial E}\Phi_\gamma(E)$ stands for the period of the orbit γ. This formula is known as the *Gutzwiller trace formula* [8]. The semiclassical approximation of the S-matrix in the present context is identical to the semiclassical T operator which was introduced by Bogomonly [22] who derived it using different considerations.

We can also apply the scattering approach to integrable systems. The integrability implies $\Phi = \Phi(E, \phi_f - \phi_i)$, since then $I_f = I_i$. Depending on whether the difference $\Delta\phi = \phi_f - \phi_i$ is a rational multiple of 2π or not, the orbit will be periodic or quasiperiodic. The ratio $\rho = \Delta\phi/2\pi$ is called the rotation number. The S-matrix in the ϕ representation is given by [21]

$$S_{sq}(E, \phi_i, \phi_f) = \left[-\frac{\partial^2 \Phi/\partial\phi_i \partial\phi_f}{2\pi \mathrm{i}}\right]^{-1/2} \exp\left[\mathrm{i}\left\{\Phi(E, \phi_f - \phi_i) - \tfrac{1}{2}\nu\pi\right\}\right] \tag{44}$$

where ν is the Maslov index for the map. From this expression, one gets the action representation by double Legendre transformation, which gives

$$S_{sq}(E, I_i, I_f) = \delta_{I_i, I_f} \exp\left[\mathrm{i}\left\{-\Delta\phi(E, I_i) I_i + \Phi(E, \Delta\phi(E, I_i)) - \tfrac{1}{2}\nu\pi\right\}\right]. \tag{45}$$

Actually, the channel quantum numbers resulting from the quantization along Γ are the integers $I_i - \nu/4$ and $I_f - \nu/4$ (recall $\hbar = 1$). As S_{sq} is diagonal in this representation, it is straightforward to compute the phase of $\operatorname{Det}\left[-S_{sq}(E)\right]$ and obtain the averaged integrated density

$$\frac{1}{2\pi}\Theta(E) = \sum_I \left[-\frac{\Delta\phi(E, I) I}{2\pi} + \frac{\Phi(E, \Delta\phi(E, I))}{2\pi} - \frac{\nu}{4}\right] - \frac{\Lambda}{2} \tag{46}$$

where we have set $I = I_i = I_f$. To evaluate $\mathrm{Tr}\, S^n_{sq}(E)$, one can use the Poisson formula

$$\sum_{n=-\infty}^{+\infty} g(n) = \int_{-\infty}^{+\infty} \mathrm{d}n \sum_{m=-\infty}^{+\infty} \mathrm{e}^{2\pi \mathrm{i} m n} g(n) \tag{47}$$

which introduces a new sum over integers m. The resulting integral is solved in the saddle-point approximation, which selects the action $\tilde{I}$ such that $\Delta\phi(E, \tilde{I}) = 2\pi m/n$. Notice that the main contributions come from the rational or periodic tori, since $\rho(\tilde{I}) \in \mathbb{Q}$. Hence we get

$$\mathrm{Tr}\, S^n_{sq}(E) = \sum_{m=-\infty}^{\infty} \left[-2\pi n \frac{\partial \Delta\phi(E, I)}{\partial I} \right]^{-1/2}_{I=\tilde{I}} \exp\left[\mathrm{i}n \left\{ \Phi\left(E, \frac{2\pi m}{n}\right) - \frac{(m+n)\nu\pi}{2} \right\} \right] \tag{48}$$

which we can now insert in (37) to obtain the semiclassical expression of the density of states.

We may check these formulae on the integrable wedge $\beta_R + \beta_L = \pi/2$, with the section $\tilde{\Gamma}$ along the inclined side (see appendix C). As this system is separable in the rotated coordinates, the rotation number is given by the ratio of the periods $T_{\tilde{x}}$ and $T_{\tilde{y}}$. The Hamiltonian in the action variables reads

$$H = H_{\tilde{x}} + H_{\tilde{y}} = \left(\frac{3\pi c}{2\sqrt{2}} I_{\tilde{x}} \right)^{2/3} + \left(\frac{3\pi s}{2\sqrt{2}} I_{\tilde{y}} \right)^{2/3} \tag{49}$$

where $I_{\tilde{x}} = \frac{1}{2\pi} \oint p_{\tilde{x}}\, \mathrm{d}\tilde{x}$ and $I_{\tilde{y}} = \frac{1}{2\pi} \oint p_{\tilde{y}}\, \mathrm{d}\tilde{y}$. The periods $T_{\tilde{x}}$ and $T_{\tilde{y}}$ are easily computed from the corresponding actions $I_{\tilde{x}}$ and $I_{\tilde{y}}$. Setting $\alpha = (2\sqrt{2}/3\pi)^{2/3}$, we get

$$\Delta\phi(E, I_{\tilde{x}}) = 2\pi \frac{c}{s} \left[\frac{E - E_{\tilde{x}}(E, I_{\tilde{x}})}{E_{\tilde{x}}(E, I_{\tilde{x}})} \right]^{1/2} = 2\pi \frac{c}{s} \left[\frac{\alpha c^{-2/3} E - I_{\tilde{x}}^{2/3}}{I_{\tilde{x}}^{2/3}} \right]^{1/2} . \tag{50}$$

Inverting this relation, one obtains the generating function of the Poincaré map on the inclined boundary $\tilde{y} = 0$:

$$\Phi(E, \Delta\phi) = \int \mathrm{d}(\Delta\phi)\, I(E, \Delta\phi) = \frac{2\pi \Delta\phi\, (\alpha E)^{3/2}}{\sqrt{(2\pi c)^2 + (s\Delta\phi)^2}} . \tag{51}$$

Replacing Φ from (51) in (44), we get

$$N_{sq}(E) \approx \frac{1}{cs} \sum_I \left[\alpha E - I^{2/3} \right]^{3/2} - \tfrac{1}{4}(\nu + 2)\Lambda \approx \frac{E^3}{12\pi sc} \tag{52}$$

as expected for this wedge, and

$$\mathrm{Tr}\, S^n_{sq}(E) \approx \sum_{m=-\infty}^{+\infty} \sqrt{\frac{3s}{c}} \frac{(\alpha E)^{3/4} (nc)^{3/2} |ms|^{1/2}}{\left(n^2c^2 + m^2s^2\right)^{5/4}} \exp\left[2\pi \mathrm{i} \left\{ \frac{(\alpha E)^{3/2} nm}{\sqrt{n^2c^2 + m^2s^2}} - \frac{(n+m)\nu}{4} + \frac{1}{8} \right\} \right] . \tag{53}$$

Substituting this expression in the second term of the RHS of (37), we obtain a semiclassical approximation for the oscillatory part of the density. Regrouping the terms with positive and negative m, one obtains a real function for real energy, which reads

$$d_{osc}(E) \approx \sum_{n,m=1}^{\infty} \sqrt{\frac{3^3}{sc}} \frac{1}{\alpha} \frac{(\alpha E)^{5/4} (nc)^{3/2} (ms)^{3/2}}{\left(n^2c^2 + m^2s^2\right)^{7/4}} \cos\left[2\pi \left\{ \frac{(\alpha E)^{3/2} nm}{\sqrt{n^2c^2 + m^2s^2}} - \frac{(n+m)\nu}{4} + \frac{1}{8} \right\} \right] . \tag{54}$$

For integrable systems it is also possible to derive the Berry–Tabor [23] semiclassical expression for $d(E)$ using EKB quantization. The EKB values for the actions are $I_1 = n_1 + \nu/4$ and $I_2 = n_2 + \nu/4$. Then, transforming both the sums into integrals using Poisson sum rule, the density reads

$$d(E) \approx \sum_{n_1,n_2=0}^{\infty} \delta\big(E - H\big[n_1 + \tfrac{1}{4}\nu, n_2 + \tfrac{1}{4}\nu\big]\big)$$

$$\approx \int_0^{\infty} \mathrm{d}I_1\, \mathrm{d}I_2 \sum_{m_1,m_2=-\infty}^{+\infty} \varphi_{m_1,m_2}(I_1, I_2)\, \delta\,(E - H\,[I_1, I_2]) \tag{55}$$

with

$$\varphi_{m_1,m_2}(I_1, I_2) = \exp\big[2\pi \mathrm{i} m_1 \big(I_1 - \tfrac{1}{4}\nu\big) + 2\pi \mathrm{i} m_2 \big(I_2 - \tfrac{1}{4}\nu\big)\big]. \tag{56}$$

The integration over $\mathrm{d}I_2$ fixes $I_2 = I_2(E, I_1)$, and the one over $\mathrm{d}I_1$ is solved in the saddle-point approximation. The term with $m_1 = m_2 = 0$ does not oscillate and hence gives the averaged density, for which we find $E^3/12\pi sc$, as before. Removing this part and regrouping the terms pairwise with respect to m_1 and m_2, we obtain exactly the same double sum as in (54).

This check provides further support for the formalism based on scattering, since the starting point of both derivations are quite different. However, the computations rely on the same methods. Except for one of the sums in (54), which comes from the expansion of the logarithm, the sums were generated by Poisson formula. In both cases, it is the saddle-point approximation which selects the contributions of the periodic tori with $\rho \in \mathbb{Q}$.

5. Numerical checks of the semiclassical analysis

In this section we discuss the applicability and the validity of the above semiclassical formula. In the numerical analysis we concentrate on the hyperbolic wedge billiard with $\beta_{\mathrm{L}} = 0$.

First we consider the Gutzwiller trace formula (43). It is important to take this formula as an equation between distributions. As we cannot observe delta distributions numerically, it will be advantageous to apply these distributions on test functions. Moreover, we have at our disposal only a finite number of eigen-energies. Test functions with strong decaying properties will be appropriate, because they will cancel the effect of the missing high eigen-energies. It has been shown that such a procedure with suitable test functions may even render the sum absolutely convergent [26]. The price for this convergence is that the delta distributions transform into peaks of finite width. A more significant check is obtained when one considers a weighted Fourier transform of this equation. The peaks should then resolve the actions of the periodic orbits. It is interesting because in this way one can detect the existence of semiclassical contributions from other kind of orbits. Broadly speaking, equation (43) shows that the periodic orbits 'know' about the eigen-energies of the quantum system. The Fourier transform tests how the quantum system 'remembers' the periodic orbits. Such a representation is usually called a length spectrum, for the actions of the Euclidean billiard are proportional to the length of the orbits.

We have seen that the angle is the only parameter influencing the dynamics. Thus, the classical system scales with energy and we have $\Phi_\gamma(E) = \phi_\gamma E^{3/2}$, where $\phi_\gamma = \Phi_\gamma(1)$. With the help of the new variable $\kappa = E^{3/2}$, we define the transformation

$$D(x) = \int_0^{\infty} \mathrm{d}\kappa \exp\left[-\left(\frac{\kappa - \kappa_0}{\Delta\kappa}\right)^2\right] \cos\left[(\kappa - \kappa_0)\, x\right] d(\kappa)\,. \tag{57}$$

As $d(\kappa)$ is known for $0 < \kappa < E_{\max}^{3/2}$, we have to chose $\Delta\kappa$ and κ_0 so that the test function almost vanishes outside this range.

While the transform of the exact density of energy is straightforward and gives

$$D(x) = \sum_n \exp\left[-\left(\frac{\kappa_n - \kappa_0}{\Delta\kappa}\right)^2\right] \cos\left[(\kappa_n - \kappa_0)x\right] \tag{58}$$

the transform of its semiclassical approximation can be computed analytically for $\kappa_0 = 0$ and well approximated for $\kappa_0 \gg \Delta\kappa$. For $\kappa_0 = 0$, i.e. when most of the weight of the test function is put around $\kappa = 0$, we obtain

$$\begin{aligned} D_{\rm sc}(x)|_{\kappa_0=0} = {} & \frac{\tan(\beta_{\rm R})}{4\pi}\frac{(\Delta\kappa)^2}{3}\left[1 - \Delta\kappa\, x\, S\left(\frac{\Delta\kappa\, x}{2}\right)\right] - \frac{1+\sec(\beta_{\rm R})}{2\sqrt{2}\pi}\frac{\Delta\kappa\sqrt{\pi}}{3} C\left(\frac{\Delta\kappa\, x}{2}\right) \\ & + \sum_\gamma \sum_{r=1}^{\infty} \frac{\phi_\gamma}{\pi} \frac{1}{\sqrt{|\mathrm{Det}[\mathbb{1} - (\partial M_\gamma)^r]|}} \frac{\sqrt{\pi}\Delta\kappa}{2} \\ & \times \left\{ \frac{\cos(r\nu_\gamma\pi/2)}{2}\left[C\left(\frac{\Delta\kappa(r\phi_\gamma + x)}{2}\right) + C\left(\frac{\Delta\kappa(r\phi_\gamma - x)}{2}\right)\right]\right. \\ & \left. + \frac{\sin(r\nu_\gamma\pi/2)}{\sqrt{\pi}}\left[S\left(\frac{\Delta\kappa(r\phi_\gamma + x)}{2}\right) + S\left(\frac{\Delta\kappa(r\phi_\gamma - x)}{2}\right)\right]\right\} \end{aligned} \tag{59}$$

where

$$C(z) = \mathrm{e}^{-z^2} \qquad \text{and} \qquad S(z) = \mathrm{e}^{-z^2}\int_0^z \mathrm{d}t\, \mathrm{e}^{t^2}. \tag{60}$$

The function $S(z)$ is known as *Dawson's integral*. Both $C(z)$ and $S(z)$ contribute to the sum mainly around $z = 0$, i.e. at $x = \pm r\phi_\gamma$, which correspond to the action of the periodic orbits and to their multiples. When $\kappa_0 \gg \Delta\kappa$, one can extend the integration over the whole κ-axis, since the contribution of the test function is then negligible for $\kappa < 0$. This gives

$$\begin{aligned} D_{\rm sc}(x)|_{\kappa_0 \gg \Delta\kappa} \approx {} & \left[\frac{\tan(\beta_{\rm R})}{4\pi}\kappa_0 - \frac{1+\sec(\beta_{\rm R})}{2\sqrt{2}\pi}\right]\frac{2\Delta\kappa\sqrt{\pi}}{3} C\left(\frac{\Delta\kappa\, x}{2}\right) \\ & + \sum_\gamma \sum_{r=1}^{\infty} \frac{\phi_\gamma}{\pi} \frac{1}{\sqrt{|\mathrm{Det}[\mathbb{1} - (\partial M_\gamma)^r]|}} \frac{\sqrt{\pi}\Delta\kappa}{2} \\ & \times \frac{\cos(r\nu_\gamma\pi/2)}{2}\left[C\left(\frac{\Delta\kappa(r\phi_\gamma + x)}{2}\right) + C\left(\frac{\Delta\kappa(r\phi_\gamma - x)}{2}\right)\right]. \end{aligned} \tag{61}$$

Figure 7 represents the Gutzwiller trace formula (43) applied on the above test function with $\kappa_0 = 0$ for the wedge with $\beta_{\rm R} = \pi/3$. The solid line is obtained from (58) with the lowest 3370 eigen-energies. A reasonable choice for the width of the Gaussian is $\Delta\kappa = 50$. The dotted line stands for the semiclassical approximation (59) with 95 periodic orbits. These are all periodic orbits with action $\phi_\gamma < 10$, except the grazing ones with $m > 13$. The actions (in units of $\hbar$) are marked with triangles. The agreement between both curves is rather good in general. One remarkable feature of the wedge billiard with $\beta_{\rm L} = 0$ and $\beta_{\rm R} > \pi/4$ is that each periodic orbit may be coded uniquely, using a two letter code. Following the orbit when starting from the inclined side, one writes a T for each bounce leading directly to the inclined side, and a V when the particle first hits the vertical side before coming back to the inclined side. This prescription is believed to lead to a different code for each periodic orbit [12]. The orbit with action $\phi_\gamma \approx 3.26$ is bouncing exactly in the corner, and hence may be coded either TTTV or TVV. As the angle is of the type π/n with $n \in \mathbb{N}^*$ and n is odd, this orbit is well defined, but the corresponding

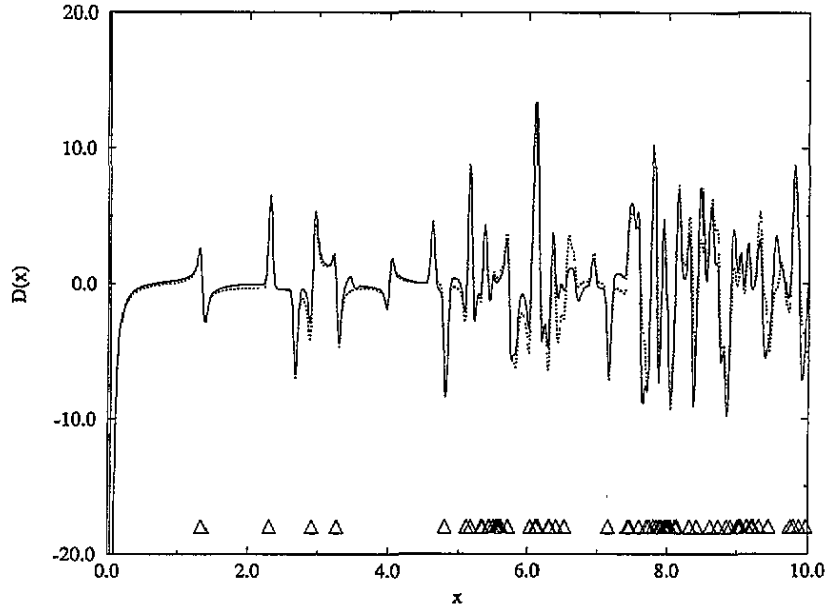

Figure 7. Action spectrum for $\beta_L = 0$, $\beta_R = \pi/3$, $\Delta\kappa = 50$ and $\kappa_0 = 0$. The full curve represents the transform of the exact density computed from 3370 levels. The dotted curve is obtained from 95 periodic orbits, whose actions are marked with triangles.

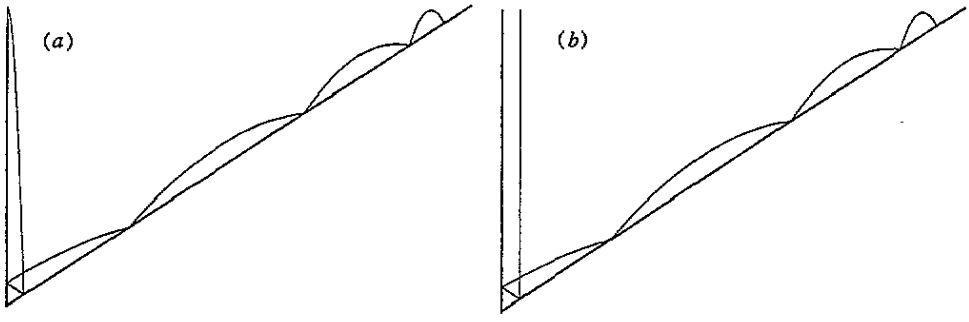

Figure 8. Families tending to an orbit running along the boundary. (*a*) Orbit of the grazing family $VVVT^m$ for $m = 6$. (*b*) Orbit of the grazing family $VTVT^m$ for $m = 6$.

monodromy matrix does not exist [25]. Perturbation of this orbit leads to either TTTV or TVV, depending on the first side hit near to the corner. So one has to derive a special saddle-point approximation which takes into account both behaviours. Following Szeredi [12], we take half the contributions of both TTTV and TVV.

A crucial assumption for the derivation of the Gutzwiller formula is that all periodic orbits are isolated and unstable. In the present case, we encounter only one problematic family of *grazing orbits* (see figure 8) which tend to a limit orbit running along the boundary. The contribution of such families is difficult to estimate, since only the first members may be considered as isolated, but not the ones near the accumulation point. Nevertheless, it has been observed on the stadium billiard [24] that adding only the contributions of a few first members well reproduces the exact density, pointing out a high cancellation phenomenon

Table 1. Asymptotic behaviour of grazing families for large m.

	$VVVT^m$	$VTVT^m$
ϕ_γ	$4\sqrt{2}(1-m^{-2}+2m^{-3})+O(m^{-5})$	$4\sqrt{2}(1-m^{-2}+2m^{-3})+O(m^{-4})$
σ_γ	-1	$+1$
μ_γ	$\log(2m^2+4m+8+O(m^{-2}))$	$\log(2m^2+4m+10+O(m^{-2}))$
ν_γ	$15+3m$	$13+3m$

between pairs of periodic orbits belonging to different grazing families.

We shall now analyse, in detail, the contribution of grazing orbits for the wedge with $\beta_R = \pi/3$ [12]. The code for the most obvious grazing family reads $VVVT^m$, where T^m means that the particle successively hits m times the inclined side without touching the vertical one. There exists another grazing family, labelled $VTVT^m$, which is a good candidate to cancel the contributions of the family $VVVT^m$ for large m. Both families tend to the same limit orbit sliding along the boundary, bouncing in the corner, going up vertically and coming back on the same path. Bouncing along the inclined boundary is integrable motion. So the map T reduces to a linear transformation in appropriate coordinates [9], and it is possible to compute analytically the exact location and the properties of both families. The behaviour of the quantities describing both grazing families is summarized in table 1, where the denominator $|\mathrm{Det}[\mathbb{1}-(\partial M_\gamma)^r]|^{-1/2}$ is characterized by σ_γ, the sign of the trace of the monodromy matrix ∂M_γ, and μ_γ, the largest eigenvalue of ∂M_γ. Notice that the limit trajectory is bouncing exactly in the vertex, where specular reflection may not be continuously defined for arbitrary angle. Here it is well defined, since the boundary is regular near the corner and the angle is of the type π/n. In contrast to what has been observed in [12], we did not find infinite families for $\beta_R = 49°$. We suspect that they may exist only when the limit orbit is well defined. The Maslov index ν_γ is extracted from numerical simulations, using the method described in [12]. Special care has to be taken when the particle bounces against the vertical wall with almost zero velocity. Out of the numerical data we found the simple rule 'add 3 for a T mapping and 5 for a V mapping'. This rule never failed on the several hundred orbits we investigated, but we have no analytical proof of it.

The main difference between both families is the way of inverting the direction of the velocity near the vertical side. Orbits of the type $VVVT^m$ hit the vertical side perpendicularly with almost zero velocity, whereas the orbits $VTVT^m$ bounce up vertically, slow down to zero velocity and come back because of the potential. This causes a difference of 2 in the Maslov index. Therefore the contributions of both families, which are very close in absolute value for large m, take opposite signs and cancel. However, this does not mean that one may consider the orbits near the accumulation point as isolated.

The situation appears to be similar in the stadium, where one grazing family bounces twice in the corner to inverse the direction of its velocity, while the other bounces perpendicularly to one side. This leads to the same difference in the Maslov indexes, and hence to cancellation of the contributions. Notice that in both cases, the grazing families are due to a part of the boundary along which motion is integrable, and the limit orbit bouncing exactly in the corner is well defined. Thus it seems that the symmetry of the dynamics near the corner plays a central role in the existence of infinite families and in the mechanism of cancellation.

The point of accumulation of grazing orbits stands at $x = 4\sqrt{2} \approx 5.65$. The excellent

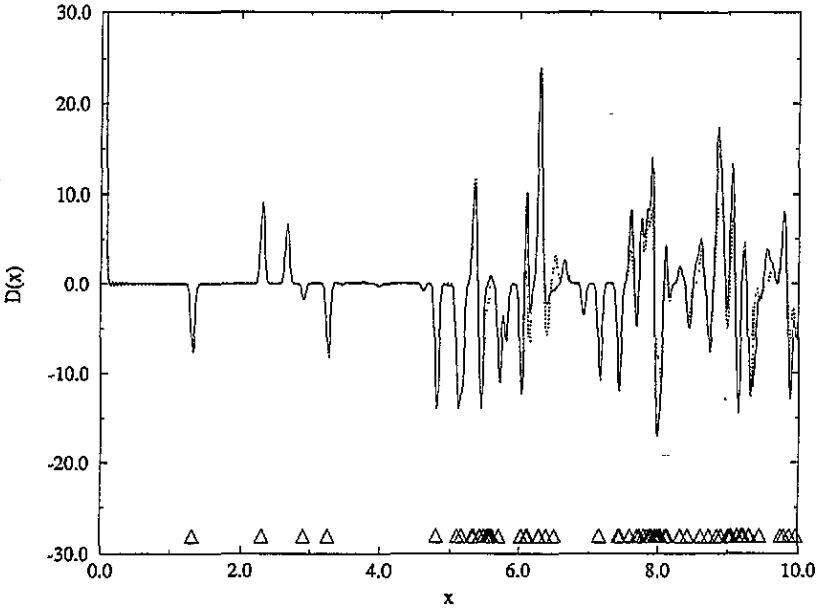

Figure 9. Action spectrum for $\beta_L = 0$, $\beta_R = \pi/3$, $\Delta\kappa = 50$ and $\kappa_0 = 150$. The full curve represents the transform of the exact density computed from 3370 levels. The dotted curve is obtained from the same 95 periodic orbits as before. The actions of the periodic orbits are marked with triangles.

matching between the curves around that point, despite the reduced number of members of the grazing families, is due to the above-described cancellation phenomenon. The other differences might originate from terms which have been neglected in the approximation (42). One cannot exclude a possible calculation error in the Maslov index, because of the difficulties involved in the numerical evaluation of some orbits. Such errors are difficult to detect when several orbits have nearly the same action.

In figure 9 we set $\kappa_0 = 150$ and used exactly the same data as before. The agreement between the curves improves significantly. This demonstrates the importance of the choice of the test function. Centring the Gaussian away from zero takes advantage of more eigen-energies, since the density of levels increases with κ. Moreover, as (43) is expected to hold in the semiclassical regime, it is natural to shift the weight to higher energies.

The Gutzwiller trace formula makes use of all periodic orbits of the classical system. Hence it is very difficult to identify the contributions of the various periodic orbits from the rest. In our derivation we obtained this formula as a sum over the traces of the powers of S_{sq}. We can therefore check the semiclassical approximation in more detail by considering the approximation (42) of $\mathrm{Tr}\, S_{sq}^n$ for each n separately. For the wedge billiard, the period n_γ represents the number of collisions with the vertical boundary, and hence corresponds to the number of V's contained in the code of the orbit. Because of the potential, each periodic orbit has to hit the vertical side at least once, so that each code contains at least one V. Thus every periodic orbit of the system contributes to one of the powers of S. Here again we are confronted with the problem of the contributions of the grazing families. For $\beta_R = \pi/3$, all members of the families VTVT^m and VVVT^m have to be included in the evaluation of $\mathrm{Tr}\, S_{sq}^2$ and $\mathrm{Tr}\, S_{sq}^3$, respectively. Here

the previous mechanism of cancellation does not apply, since both families contribute to separate quantities. However, as the Maslov index steadily increases by 3 for each member of the same family, contributions from consecutive members (considered here as separated) will have different phases so that the whole sum will converge at the end.

For the same reasons discussed above, we calculate a weighted Fourier transform of $\mathrm{Tr}\, S^n_{\mathrm{sq}}(\kappa)$:

$$T^n(x) = \int_0^\infty \mathrm{d}\kappa\, \exp\left[-\left(\frac{\kappa-\kappa_0}{\Delta\kappa}\right)^2\right] \exp\left[\mathrm{i}\kappa x\right]\, \mathrm{Tr}\, S^n(\kappa). \tag{62}$$

The semiclassical approximations with $\kappa_0 = 0$ and $\kappa_0 \gg \Delta\kappa$ read

$$T^n_{\mathrm{sc}}(x)|_{\kappa_0=0} = \sum_{\{\gamma\,|\,n_\gamma r_\gamma = n\}} \frac{n_\gamma}{\sqrt{|\mathrm{Det}[\mathbb{1} - (\partial M_\gamma)^{r_\gamma}]|}} \Delta\kappa\, \exp\left[-\mathrm{i} r_\gamma \nu_\gamma \frac{\pi}{2}\right]$$
$$\times \left[\frac{\sqrt{\pi}}{2} C\left(\frac{\Delta\kappa(r_\gamma\phi_\gamma - x)}{2}\right) + \mathrm{i}S\left(\frac{\Delta\kappa(r_\gamma\phi_\gamma - x)}{2}\right)\right] \tag{63}$$

$$T^n_{\mathrm{sc}}(x)|_{\kappa_0 \gg \Delta\kappa} \approx \sum_{\{\gamma\,|\,n_\gamma r_\gamma = n\}} \frac{n_\gamma}{\sqrt{|\mathrm{Det}[\mathbb{1} - (\partial M_\gamma)^{r_\gamma}]|}} \Delta\kappa\sqrt{\pi}$$
$$\times \exp\left[\mathrm{i} r_\gamma\left(\phi_\gamma - \tfrac{1}{2}\nu_\gamma\pi\right) - \mathrm{i}\kappa_0 x\right] C\left(\tfrac{1}{2}\Delta\kappa(r_\gamma\phi_\gamma - x)\right). \tag{64}$$

We shall present results which are calculated for the semiclassical domain $\kappa_0 \gg \Delta\kappa$. Figure 10 represents the real part of the transform for $n = 1$ and $\kappa_0 = 150$. The full curve stands for $T^1(x)$. It is obtained from the discrete Fourier transform of 900 values with κ between 0 and 332. The dotted line represents $T^1_{\mathrm{sc}}(x)|_{\kappa_0 \gg \Delta\kappa}$. It is computed from

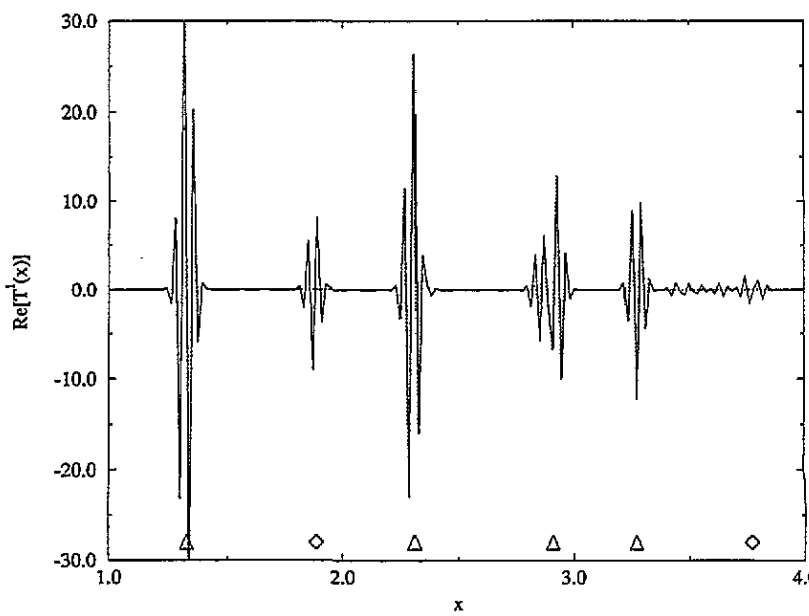

Figure 10. Real part of the action spectrum of $\mathrm{Tr}\, S_{\mathrm{sq}}$ for $\beta_{\mathrm{L}} = 0$, $\beta_{\mathrm{R}} = \pi/3$, $\Delta\kappa = 50$ and $\kappa_0 = 150$. The full curve represents the transform of the semiquantal expression. The dotted line is obtained from the periodic orbits bouncing only once against the vertical wall. The contributions due to the onset of new channels are marked with diamonds.

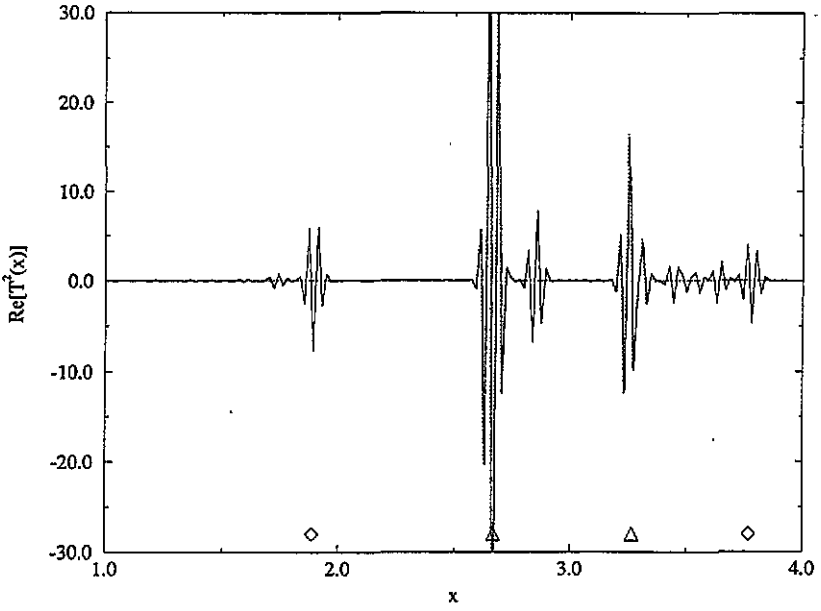

Figure 11. Real part of the action spectrum of $\mathrm{Tr}\,S_{sq}^2$ for $\beta_L = 0$, $\beta_R = \pi/3$, $\Delta\kappa = 50$ and $\kappa_0 = 150$. The full curve represents the transform of the semiquantal expression. The dotted curve is obtained from two periodic orbits bouncing twice against the vertical wall. The contributions due to the onset of new channels are marked with diamonds.

all periodic orbits bouncing only one time against the vertical wall. The actions of these four orbits are marked with triangles. The semiclassical approximation perfectly matches the exact curve around the periodic orbits. For the same reason as before, we take half the contribution of the orbit TTTV. Here the process is obvious, since TVV does not contribute to this sum. Apart from the large peaks which appear at the location of periodic orbits, there are also other peaks at multiples of $4\sqrt{2}/3 \approx 1.88$ (marked with diamonds). We have made certain that these peaks are due to the periodicity induced by the onset of new thresholds. There are other factors which cannot be accounted for by either the simple assumption about the onset of thresholds or by the semiclassical theory. They are yet unexplained.

In figures 11 and 12 we plot $T^2(x)$ and $T_{sc}^2(x)|_{\kappa_0 \gg \Delta\kappa}$ on a range including all periodic orbits bouncing twice against the vertical wall. The dotted line results from five isolated periodic orbits and from the first 10 members of the family VTVT^m. The semiclassical approximation reproduces the behaviour of $T^2(x)$ near the accumulation point at $x \approx 5.65$ well, pointing out the proper mechanism of cancellation of this family.

The traces of the powers of S give the semiclassical approximation of the oscillatory part of $d(E)$. It is also easy to check the formula for the averaged density via (40), which gives an approximation of the integrated averaged density as a quantity depending on the S. The full curve in figure 13 represents the exact integrated density $N(E)$ for the range of energy where $\Lambda(E) = 40$ and $\beta_R = \pi/3$. The dotted curve is computed from the variation of the phase of $\mathrm{Det}(-S)$ divided by 2π and stands for the semiclassical approximation of $N_{AV}(E)$.

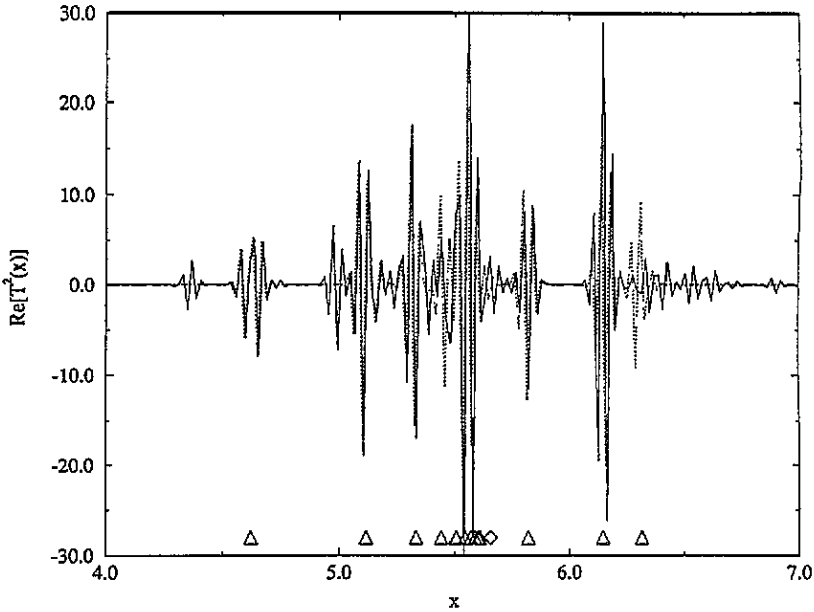

Figure 12. Real part of the action spectrum of $\mathrm{Tr}\,S_{sq}^2$ for $\beta_L = 0$, $\beta_R = \pi/3$, $\Delta\kappa = 50$ and $\kappa_0 = 150$. The full curve represents the transform of the semiquantal expression. The dotted curve is obtained from the periodic orbits bouncing twice against the vertical wall and the lowest 10 members of the grazing family VTVT^m. The contributions due to the onset of new channels are marked with diamonds.

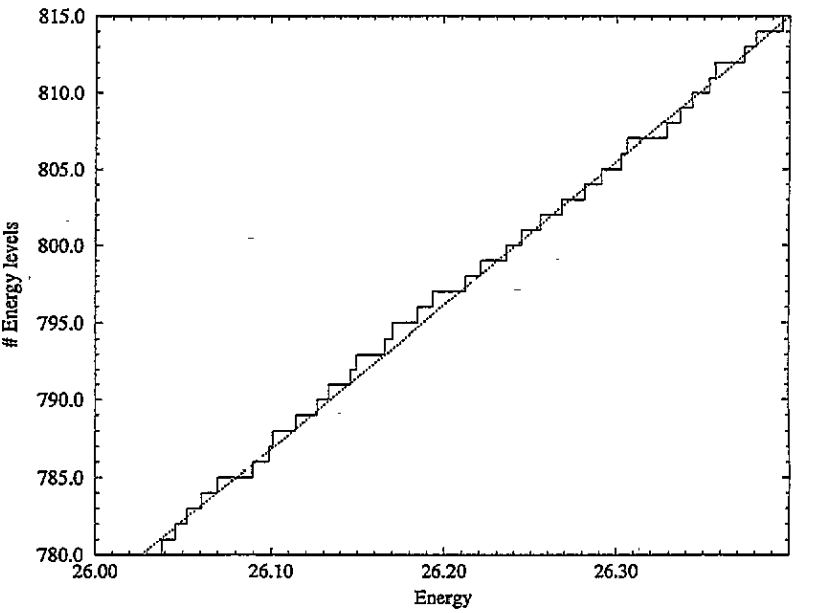

Figure 13. Integrated density of energy for $\beta_L = 0$, $\beta_R = \pi/3$ and E such that $\Lambda(E) = 40$. The full curve represents the exact integrated density $N(E)$. The dotted line is obtained from the phase of $\mathrm{Det}(-S)$ divided by 2π and stands for the semiclassical approximation of $N_{\mathrm{AV}}(E)$.

6. Discussion

In this paper we have extended the scattering approach to quantization to include not only billiards, but also smooth Hamiltonians of the type (1). The method was applied to the wedge billiard which falls into the class of 'inclined billiards' where the motion between successive bounces is not free. We have shown that the general formalism can also be applied to the present system.

The scattering approach has a few advantages: the quantization condition is formulated as a secular equation which requires that, at an eigen-energy, the spectrum of the extended S-matrix includes the value 1. Restricting the S-matrix to the space of opened channels, and proceeding with the semiclassical approximation, we were able to derive not only the Gutzwiller trace formula for chaotic and integrable systems, but also to calculate the leading terms for the smooth level density. The fundamental step in the semiclassical approximation is the calculation of $\mathrm{Tr}\, S^n$ in terms of periodic orbits of the classical Poincaré scattering map. We could test the accuracy of this approximation numerically, and found a very good agreement. The scattering approach is a very convenient numerical tool. In the present work we were able to calculate thousands of eigenvalues of the wedge billiard with a very high accuracy. Using this database, we could check various aspects of the semiclassical theory, which were not accessible to previous authors who had to perform their analysis in terms of numerical spectra which are poorer both in accuracy and number of levels. We could, for example, test the role of families of periodic orbits which converge to a limit orbit.

There are a few points in the scattering approach which need further elucidation. The first has to do with the condition which is the basis of the method, namely, that an eigenvalue occurs whenever the extended $S(E)$-matrix has 1 as an eigenvalue. This is a condition which is well defined for any finite truncation of the extended S-matrix, but may be problematic when the full S operator is considered. A difficulty of this sort occurs in the alternative method which uses the exterior–interior duality for the quantization of billiards [3]. There it was shown by Eckmann and Pillet [7] that the condition for quantization has to be understood as a limit, so that as $E \nearrow E_n$ one eigenphase of the S-matrix approaches 1 from above. In the present variant of the scattering approach, other complications may arise. The extended S-matrix is not unitary, and at threshold energies it is not even analytic in the energy E. We observed numerically that, between thresholds, the spectrum of the extended S-matrix is composed of A eigenvalues which are in the close vicinity of the unit circle, and the rest, which are concentrated near 0. As a threshold is approached, the absolute value of one of the eigenvalues near 0 starts to increase and at the threshold energy it reaches the unit circle through the vicinity of 1. This occurrence of the value 1 in the spectrum does not signal the appearance of a new eigen-energy of the system. Rather, it is a consequence of the opening of a new channel. In figure 14 we trace the dependence of the eigenvalues of the S-matrix near a threshold. We are not able to provide an explanation for the observed behaviour, but is seems to be universal (see, for example, a similar figure in [6]), and therefore essential for the complete understanding of the scattering approach.

Because of lack of space, we did not report in this paper about some of our numerical and analytical studies which relate to the spectral statistics, spectral correlations and the distribution of spectral 'velocities' $\partial E_n/\partial\beta$. These distributions and correlations are now studied with applications to atomic and mesoscopic physics. The extensive data set that we built for the wedge billiard offers an excellent basis for such statistical studies, which will be reported in a subsequent publication.

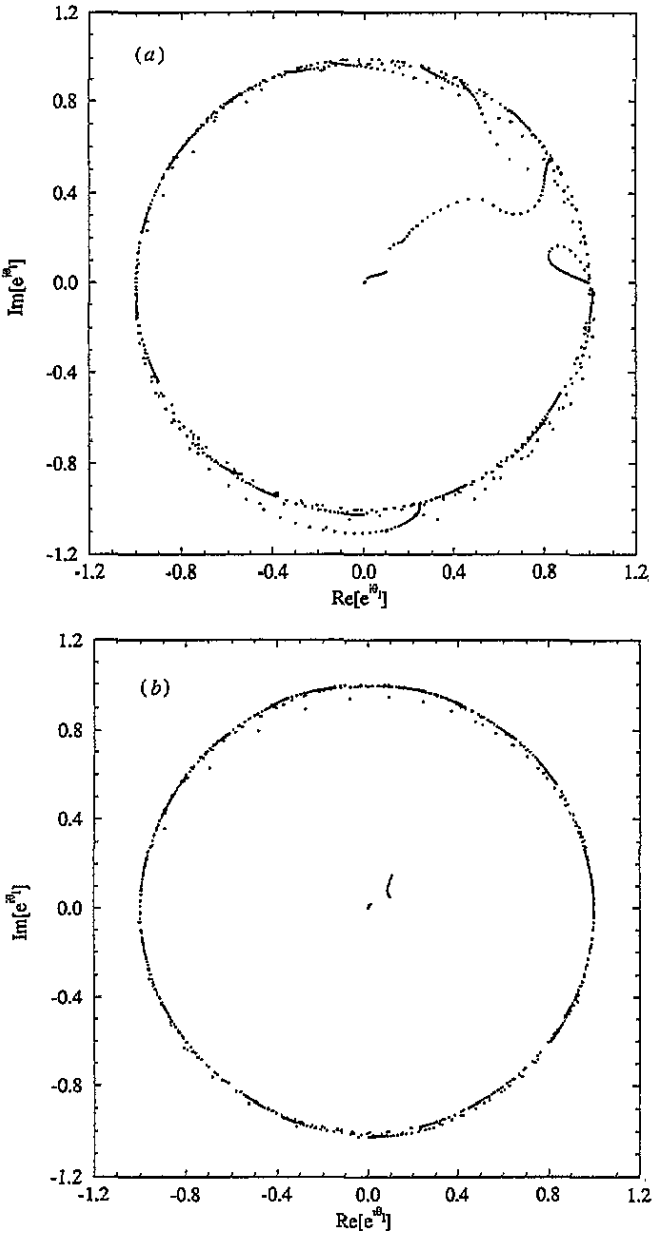

Figure 14. Parametric representations of the 25 first eigenphases $e^{i\theta_l}$ as a function of the energy for $\beta_L = 0$ and $\beta_R = \pi/3$ near a threshold. The energy parameter runs from 10 units of the mean level spacing below the 21st threshold to 10 units above. (*a*) Energy interval below the threshold. The energy difference between the dots is chosen to decrease exponentially. (*b*) Energy interval above the threshold. Here the energy difference between the circles increases exponentially.

Acknowledgments

We are grateful to H Schanz for fruitful discussions on various aspects of this work, particularly on the symmetries of the *S*-matrix. CR wish to thank Ph Choquard, M Cibils

and T Dagaeff for stimulating discussions. US is obliged to the theoretical physics group at the Ecole Polytechnique Fédérale de Lausanne for the hospitality extended to him during his stay. US acknowledges partial support from the Minerva Center for Nonlinear Physics of Complex Systems. We wish to thank T Dagaeff and H Primack for valuable comments on the manuscript.

Appendix A. Symmetries of the S-matrix

In this appendix, we show the consequences of invariance with respect to time inversion and reality of the potential on the structure of the scattering matrix. These relations may also be derived by combining other equations [6], but their origin lies in the above symmetry. They provide an easy proof of the symmetry of the full S-matrix and are useful for verifying the accuracy of the numerical computations.

To improve the formulation of the results, we will use the notation

$$S = \begin{pmatrix} S_{oo} & S_{oc} \\ S_{co} & S_{cc} \end{pmatrix} \tag{A1}$$

where the indexes o and c of the submatrices stand respectively for *open* and *closed* channels. This notation has to be taken with some care, since $(S^{T})_{oc} = (S_{co})^{T}$.

As the potential is real and time-independent, ψ and ψ^* are both solutions of the same Schrödinger equation. Choosing a wavefunction ψ as a linear combination of the ψ_n involving no incoming closed modes and decomposing it into sums of propagating and non-propagating modes, we obtain

$$\psi = \sum_{n=1}^{\Lambda} a_n \psi_n = \sum_{n=1}^{\Lambda} a_n \frac{1}{\sqrt{k_n}} e^{ik_n x} \phi_n(y) + \sum_{l=1}^{\Lambda} b_l \frac{1}{\sqrt{k_l}} e^{-ik_l x} \phi_l(y) + \sum_{l=\Lambda+1}^{\infty} b_l \frac{1-i}{\sqrt{2\kappa_l}} e^{\kappa_l x} \phi_l(y) \tag{A2}$$

where $\kappa_l = \sqrt{|E - E_l|}$. The coefficients of the outgoing modes satisfy $b_l = \sum_{n=1}^{\Lambda} a_n S_{nl}$. The complex conjugate then reads

$$\psi^* = \sum_{n=1}^{\Lambda} a_n^* \psi_n^* = \sum_{l=1}^{\Lambda} b_l^* \frac{1}{\sqrt{k_l}} e^{ik_l x} \phi_l(y) + \sum_{n=1}^{\Lambda} a_n^* \frac{1}{\sqrt{k_n}} e^{-ik_n x} \phi_n(y) + \sum_{l=\Lambda+1}^{\infty} i b_l^* \frac{1-i}{\sqrt{2\kappa_l}} e^{\kappa_l x} \phi_l(y) . \tag{A3}$$

As a solution of the scattering system, the coefficients of the outgoing modes may also be related to the ingoing ones via the S-matrix

$$a_n^* = \sum_{l=1}^{\Lambda} b_l^* S_{ln} \qquad \text{for} \quad n \leqslant \Lambda \tag{A4}$$

$$i b_l^* = \sum_{m=1}^{\Lambda} b_m^* S_{ml} \qquad \text{for} \quad l > \Lambda . \tag{A5}$$

Inserting the definition of b_l in both relations, and noting that they are valid for any choice of the coefficients a_n, we obtain

$$\sum_{l=1}^{\Lambda} S_{ml}^* S_{ln} = \delta_{mn} \qquad \text{for} \quad n, m \leqslant \Lambda \tag{A6}$$

$$i S_{nl}^* = \sum_{m=1}^{\Lambda} S_{nm}^* S_{ml} \qquad \text{for} \quad n \leqslant \Lambda \quad \text{and} \quad l > \Lambda . \tag{A7}$$

Similarly, choosing ψ with no incoming open modes gives

$$\sum_{m=1}^{\Lambda} S_{nm}^{*} S_{ml} = \mathrm{i}(S_{nl}^{*} - S_{nl}) = 2\,\mathrm{Im}\,[S_{nl}] \qquad \text{for} \quad n, l > \Lambda\,. \tag{A8}$$

Using compact notation, these relations read

$$S_{oo} \cdot S_{oo}^{*} = S_{oo}^{*} \cdot S_{oo} = \mathbb{1} \tag{A9}$$

$$S_{oo} \cdot S_{oc}^{*} = -\mathrm{i} S_{oc} \tag{A10}$$

$$S_{co} \cdot S_{oc}^{*} = \mathrm{i}\left(S_{cc}^{*} - S_{cc}\right) = 2\mathrm{Im}\,[S_{cc}]\,. \tag{A11}$$

The divergence of the current vanishes for stationary states of the Schrödinger equation with real potential. Thus the flux $F(x)$ through the surface delimited by the right (left) part of the system and the section Γ at $x =$ constant must also vanish. The only part which contributes is the section Γ, so that

$$F(x) = \frac{1}{2\mathrm{i}} \int_{-\infty}^{\infty} \mathrm{d}y (\psi^{*} \nabla_x \psi - \psi \nabla_x \psi^{*})\,. \tag{A12}$$

Requiring $\Phi(x)$ to be zero successively for wavefunctions ψ with no incoming closed modes, no incoming open modes and finally both incoming closed and open modes yields

$$S_{oo} \cdot S_{oo}^{\dagger} = S_{oo}^{\dagger} \cdot S_{oo} = \mathbb{1} \tag{A13}$$

$$S_{oo} \cdot S_{oc}^{\dagger} = -\mathrm{i} S_{oc} \tag{A14}$$

$$S_{co} \cdot S_{oc}^{\dagger} = \mathrm{i}\left(S_{cc}^{\dagger} - S_{cc}\right). \tag{A15}$$

Comparing pairwise both sets of equations, we get $S = S^{\mathrm{T}}$. Thus the symmetry of the total S-matrix is a consequence of the fact that the potential is time-independent and real.

Appendix B. One-dimensional quantum bouncer

The differential equation and boundary condition for the wavefunction $\phi(x)$ of a one-dimensional particle confined between a hard wall and a gravitational potential reads

$$\begin{aligned} &\frac{\mathrm{d}^2\phi}{\mathrm{d}x^2} + \frac{2m^2 g}{\hbar^2}\left(\frac{E}{mg} - x\right)\phi = 0 \qquad && \text{if} \quad x > 0 \\ &\phi = 0 && \text{if} \quad x \leqslant 0\,. \end{aligned} \tag{B1}$$

Using the variable substitution $z = (2m^2 g/\hbar^2)^{1/3}(x - E_n/mg)$, the differential equation transforms into (see [27])

$$\frac{\mathrm{d}^2\phi}{\mathrm{d}z^2} - z\phi = 0. \tag{B2}$$

As a second-order differential equation, this latter admits two linear independent solutions $\mathrm{Ai}(z)$ and $\mathrm{Bi}(z)$ which are called *Airy functions*. The wavefunction must be bounded for $x \to +\infty$, thus $\mathrm{Bi}(z)$ has to be excluded. The solutions then take the form

$$\phi(x) = c\,\mathrm{Ai}\left[\left(\frac{2m^2 g}{\hbar^2}\right)^{1/3}\left(x - \frac{E}{mg}\right)\right] \tag{B3}$$

with c the normalization constant. Setting $\phi(0) = 0$ quantizes the energy, which then takes the values

$$E_n = -\left(\frac{2m^2 g}{\hbar^2}\right)^{-1/3} mg z_n \qquad \text{for} \quad n \in \mathbb{N}^{*} \tag{B4}$$

where z_n is the nth zero of $\mathrm{Ai}(z)$. It is straightforward to compute the normalization constant c_n:

$$\begin{aligned}\|\phi_n\|^2 &= c_n^2\left(\frac{2m^2g}{\hbar^2}\right)^{-1/3}\int_{z_n}^{\infty}\mathrm{Ai}^2(z)\,\mathrm{d}z \\ &= c_n^2\left(\frac{2m^2g}{\hbar^2}\right)^{-1/3}\left|z\mathrm{Ai}^2(z)-\mathrm{Ai}'^2(z)\right|_{z_n}^{\infty} \\ &= c_n^2\left(\frac{2m^2g}{\hbar^2}\right)^{-1/3}\mathrm{Ai}'^2(z_n)\,. \end{aligned} \tag{B5}$$

Thus the orthonormal set of eigenfunctions reads

$$\phi_n(x)=\left(\frac{2m^2g}{\hbar^2}\right)^{1/6}\frac{1}{\mathrm{Ai}'(z_n)}\,\mathrm{Ai}\left[\left(\frac{2m^2g}{\hbar^2}\right)^{1/3}\left(x-\frac{E_n}{mg}\right)\right] \qquad \text{for} \quad n\in\mathbb{N}^*\,. \tag{B6}$$

Appendix C. Integrable case with the section on the inclined boundary

Here we discuss the integrable case $\beta_{\mathrm{L}}+\beta_{\mathrm{R}}=\pi/2$, assuming that the section $\tilde{\Gamma}$ is taken on the side $\tilde{y}=0$ (see figure 8). The potential in the waveguide is defined by the value of the original potential on the $\tilde{x}$-axis. Hence it is also linear, but directed towards the $\tilde{x}$-direction. The channel eigenfunctions $\tilde{\phi}_n(\tilde{x})$ and eigen-energies $\tilde{E}_n$ are taken from appendix B with $\tilde{g}=g\cos(\beta_{\mathrm{R}})$. The scattering functions $\tilde{\psi}_m^{\mathrm{R}}$ are decomposed on the basis

$$\tilde{\varphi}_r=\mathrm{Ai}\left[(2c)^{1/3}\tilde{x}+z_r\right]\mathrm{Ai}\left[(2s)^{1/3}\tilde{y}-(2^{1/3}E+c^{2/3}z_r)s^{-2/3}\right] \qquad \text{with} \quad r\in\mathbb{N}^*. \tag{C1}$$

The matrix $\tilde{S}^{\mathrm{L}}=-\mathbb{1}$, and $\tilde{S}^{\mathrm{R}}$ is determined by the matching condition at $\tilde{y}=0$. Computation of $\tilde{I}^1_{mn}(E)$ at the eigen-energies $E_{ml}=-2^{-1/3}(c^{2/3}z_m+s^{2/3}z_l)$ yields

$$\tilde{I}^1_{mn}(E_{ml})=0 \qquad \forall n\in\mathbb{N}^*. \tag{C2}$$

Thus the kernel of $\left[\tilde{I}^1(E_{ml})\right]^{\mathrm{T}}$ admits the expected non-trivial solution

$$\left.\begin{array}{ll} b_m & \neq 0 \\ b_i & =0 \qquad \text{for} \quad i\neq m \end{array}\right\} \quad\Rightarrow\quad \Psi(x,y)=\tilde{\varphi}_m(x,y)\,. \tag{C3}$$

Notice that, although it would give the correct result, the choice Γ on $x=0$ is inappropriate for this investigation. This shows that for symmetry reasons it may be advantageous to take the section at different places.

Note added. A similar approach in terms of propagators has been developed recently by Prosen [28].

References

[1] Doron E and Smilansky U 1992 Semiclassical quantization of chaotic billiards: a scattering approach *Nonlinearity* **5** 1055

[2] Smilansky U 1992 Semiclassical quantization of chaotic billiards *Chaos and Quantum Chaos* ed W Dieter Heiss (Berlin: Springer)

[3] Dietz B and Smilansky U 1993 A scattering approach to the quantization of billiards—the inside/outside duality *Chaos* **3** 581

[4] Gutzwiller M C 1993 Poincare surface of section and quantum mechanics *Chaos* **3** 591

[5] Dietz B and Smilansky U 1993 Scattering from a square obstacle *Preprint* Weizmann Institute

[6] Schanz H and Smilansky U 1993 Quantization of Sinai's billiard—a scattering approach *Preprint* Weizmann Institute

[7] Eckmann J P and Pillet C A 1994 Spectral duality for planar billiard *Preprint* University of Geneva

[8] Gutzwiller M C 1990 *Chaos in Classical and Quantum Mechanics* (New York: Springer)
[9] Richter P H, Scholz H J and Wittek A 1990 A breathing chaos *Nonlinearity* **3** 45
[10] Wittek A 1991 Die Quantenmechanik eines nichtintegrablen Systems *PhD Thesis* Universität Bremen
[11] Szeredi T and Goodings D A 1992 Periodic orbits from the quantum energy spectrum of the wedge billiard *Phys. Rev. Lett.* **69** 1640
[12] Szeredi T and Goodings D A 1993 Classical and quantum chaos in the wedge billiard: classical mechanics *Phys. Rev. E* **48** 3518
[13] Szeredi T and Goodings D A 1993 Classical and quantum chaos in the wedge billiard: quantum mechanics and quantization rules *Phys. Rev.* E **48** 3529
[14] Szeredi T, Lefebvre J H and Goodings D A 1993 Application of bogomonly transfer operator to semiclassical quantization of chaotic systems *Phys. Rev. Lett.* **71** 2891
[15] Wojtkowski M P 1990 A system of one dimensional balls with gravity *Commun. Math. Phys.* **126** 507
[16] Abramowitz M and Stegun I A 1964 *Handbook of Mathematical Functions* (New York: Dover)
[17] Goldberger M L and Watson K M 1964 *Collision Theory* (New York: Wiley)
[18] Jung C 1986 Poincaré map for scattering states *J. Phys. A: Math. Gen.* **19** 1345
[19] Blümel R and Smilansky U 1990 Random-matrix description of chaotic scattering: semiclassical approach *Phys. Rev. Lett.* **64** 241
[20] Creagh S C, Robbins J M and Littlejohn R G 1990 Geometrical properties of Maslov indices in the semiclassical trace formula for the density of states *Phys. Rev.* A **42** 1907
[21] Miller W H 1974 Classical-limit quantum mechanics and the theory of molecular collisions *Adv. Chem. Phys.* **25** 69
[22] Bogomonly E B 1992 Semiclassical quantization of multidimensional systems *Nonlinearity* **5** 805
[23] Berry M V and Tabor M 1976 Closed orbits and the regular bound spectrum *Proc. R. Soc.* A **349** 101
[24] Sieber M, Smilansky U, Creagh S C and Littlejohn R G 1993 Non-generic spectral statistics in the quantized stadium billiard *J. Phys. A: Math. Gen.* **26** 6217
[25] Dagaeff T and Rouvinez C 1993 On the Discontinuities of the boundary in billiards *Physica* D **67** 166
[26] Sieber M and Steiner F 1990 Generalized periodic orbit sum rules for strongly chaotic systems *Phys. Lett.* **144A** 159
[27] Landau L D and Lifshitz E M 1958 *Quantum Mechanics: Non-Relativistic Theory* (Oxford: Pergamon)
[28] Prosen T 1994 Exact quantum surface of section method *Preprint* CAMTP/94-7